

# Accepted manuscript doi: 10.1680/jgein.22.00352

---

## **Accepted manuscript**

As a service to our authors and readers, we are putting peer-reviewed accepted manuscripts (AM) online, in the Ahead of Print section of each journal web page, shortly after acceptance.

## **Disclaimer**

The AM is yet to be copyedited and formatted in journal house style but can still be read and referenced by quoting its unique reference number, the digital object identifier (DOI). Once the AM has been typeset, an ‘uncorrected proof’ PDF will replace the ‘accepted manuscript’ PDF. These formatted articles may still be corrected by the authors. During the Production process, errors may be discovered which could affect the content, and all legal disclaimers that apply to the journal relate to these versions also.

## **Version of record**

The final edited article will be published in PDF and HTML and will contain all author corrections and is considered the version of record. Authors wishing to reference an article published Ahead of Print should quote its DOI. When an issue becomes available, queuing Ahead of Print articles will move to that issue’s Table of Contents. When the article is published in a journal issue, the full reference should be cited in addition to the DOI.

# Accepted manuscript doi: 10.1680/jgein.22.00352

---

**Submitted:** 08 September 2022

**Published online in 'accepted manuscript' format:** 06 October 2022

**Manuscript title:** Digital image-based Performance evaluation of GCL-sand interfaces under repeated shearing

**Authors:** Anjali G. Pillai and Madhavi Latha Gali

**Affiliation:** Department of Civil Engineering, Indian Institute of Science, Bangalore, India

**Corresponding author:** Madhavi Latha Gali, Department of Civil Engineering, Indian Institute of Science, Bangalore – 560012, India.

**E-mail:** madhavi@iisc.ac.in

## **Abstract**

Inadequate shear strength mobilization at the interfaces results in translational failures in Geosynthetic Clay Liners (GCL). Periodic addition of solid waste into the landfill causes additional normal and shear stresses in GCLs. The mechanical response of GCLs is highly time dependent and over the time, the quality and strength of fibres of GCL deteriorate. Hence the interface shear resistance reduces under the application of repeated shear cycles. To simulate these conditions, a repeated interface shearing test was conceptualized in this study. A natural river sand and a manufactured sand of identical gradation were used in experiments to understand the effects of particle shape on interface shear strength variation under repeated shearing. Each GCL-sand interface was subjected to eight cycles of shearing in dry and hydrated conditions under three different static normal stresses. Results showed that the variation of the peak interface shear stress has different phases, governed by different mechanisms. Digital image analysis of tested GCL surfaces after each shearing cycle provided important clues for this response. Entrapment of sand particles into GCL surface is beneficial initially because of increased friction at the interface and this benefit is more pronounced in case of manufactured sand, due to the irregular shape of particles. After a few shearing cycles, the fibres of the GCL got ruptured due to repeated rubbing of sand particles, which reduced the shearing resistance. Quantification of sand particle entrapment and surface changes to GCL helped in understanding these micro-level interaction mechanisms.

**Keywords:** Geosynthetics, Interfaces, geosynthetic clay liner, repeated loading, digital image analysis, UN SDG 12: Responsible consumption and production

## Introduction

Engineered landfills are integral parts of efficient waste management systems. They facilitate safe disposal of unwanted, toxic, and hazardous substances which otherwise disperse into the environment, leading to harmful consequences (Touze et al., 2006). These waste disposal facilities are lined and covered to arrest the leakage of wastewater and harmful gases into the atmosphere and ground water. The design of landfill lining system has undergone several changes over the last few decades and evolved progressively to ensure efficient waste containment (Booker et al., 2004; Hou et al., 2018). The bottom lining system of a landfill arrests the migration of contaminants and is required to prevent pollution of soil or groundwater. In earlier days, landfill liners were made using natural geological materials of low permeability. The technique of using polymers in landfill lining systems has brought revolutionary developments in this field. Geosynthetic Clay Liners (GCL) have rapidly evolved as efficient containment systems in landfill constructions. GCL is defined as a hydraulic barrier formed with a layer of bentonite sandwiched between two geosynthetic layers or attached to a geomembrane, used for preventing the migration of leachate from the landfill. GCLs provide excellent protection against leakage, apart from being economical and highly tolerant to strains and cracking compared to clay barriers.

Slope stability is of concern when the engineered landfills are built over sites with inadequate soil layer thickness or layers of low shear strength. Restrictions on the availability of land necessitate steeper slopes for landfill lining systems. GCLs have comparatively lesser interface shear resistance compared to compacted clay liners and the post-peak reduction in interface shear strength in GCLs is relatively high (Gilbert et al., 1996). Translational failure triggered by inadequate interface shear resistance and slippage between GCL and soil subgrade is identified as one of the leading causes of landfill instability in several studies (Koerner and Soong, 2000; Bergado et al., 2006). Further, vertical expansion of existing landfills by building new landfills on the side slopes of older ones increases the possibility of translational failures (Tano et al., 2015). Hence precise quantification of shear resistance of GCL interfaces is very important for the stability computations of landfills. Direct shear tests and ring shear tests are conventionally used by researchers to measure the interface shear parameters in laboratory. As specified by ASTM D 6243, the direct shear box test involves application of translational shear displacement at the interface at a constant rate to assess the interface shear strength parameters (Stoltz and Herault, 2014). Two major limitations of this test are the non-uniform stress conditions within the soil specimen because of the change in contact area during shearing and difficulties in correct assessment of interface residual shear strength due to limited shear displacement (Fox et al., 1997). The

constraints on large displacement testing in direct shear testing are overcome in ring shear tests. In a ring shear test, rotational displacement is applied to a ring-shaped soil specimen with the geosynthetic carriers of the GCL wrapped around it while the specimen rotates about its central axis. Though this test eliminates the errors in contact area and residual strength measurements, it suffers from boundary effects and complex testing requirements (Lupini et al. 1981). Some researchers have carried out inclined plane tests on GCL interfaces in which shear stress is induced by the weight of the soil and resistance offered by the interface to sliding is quantified (Reyes-Ramirez and Gourc, 2003; Pitanga et al., 2009). Like direct shear tests, measurement of interface residual shear strength parameters is not possible in inclined plane tests. Literature suggests that most of the existing test procedures fall short in simulating field conditions such as GCL hydration, variations in temperature, seismic loading, and repeated shearing conditions through laboratory tests.

While GCLs are being extensively used in baseliner and cover systems of landfills, ensuring adequate internal and interfacial shear strength has become a matter of paramount importance in the design of these systems. Variation of interface shear strength of nonwoven and woven geotextile layers of GCL with geomembrane, geonet and clayey soil was extensively investigated in literature (Rowe and Orsini, 2003; Chang et al., 2021). Several other studies highlighted the role of bentonite on the internal shear strength of GCL as bentonite in GCL hydrates and expands, causing tension on the reinforcing needle-punched fibres (Zanzinger, 2016; McCartney et al., 2009). The swollen bentonite reduces the internal shear strength and causes slip at the interface. The failures of Kettleman Hills landfill in 1988, Mahoning landfill in 1996 and Chrin Brothers landfill in 2013 in USA are attributed to the slippage between the waste mass and liner interface, leading to catastrophic damages (Stark et al., 1998; Bonaparte et al., 2020). In Kettleman Hills landfill, a composite base liner with a smooth geomembrane overlying compacted clay was used, which triggered easy slippage of waste mass over the interface. In Mahoning landfill, an unreinforced GCL with geomembrane was used as the liner. Large shear displacements in the GCL due to the settlement of waste caused interface shear failure because of low residual strength conditions. The reason for the failure of Chrin Brothers landfill was inadequate shear strength of the bottom geosynthetic liner system. Many earlier studies had highlighted the importance of adequate interface friction of the lining systems for the stability of landfills. Failure of the landfill becomes imminent if the slope stability aspects are not completely considered in the design (Blight 2007; Stark et al., 2008; Wu et al., 2008; Zornberg, 2009; Eid 2011). Literature suggests that GCLs with reinforcement in the form of needle-punched internal fibres possess high interface shear strength and withstand failures. The high magnitude shear stresses in

GCL are counteracted by the tensile forces developed in reinforcing fibres, which helps them in sustaining through critical conditions like bentonite hydration and earthquakes (Bouazza, 2002). Many researchers have demonstrated the high shearing resistance of needle punched GCLs through direct shear tests (Siebken et al., 1997; Olsta and Swan, 2001; Fox et al. 1997; Feng et al., 2020). These studies showed that the strength of a GCL depends on the strength of the geotextile material and the connection between the needle punch and the geotextile. The internal peak and residual shear strengths of the GCL were also found to be influenced by the pore pressure and pullout of the fibres (Fox et al. 2015; Fox and Stark, 2015). Bacas et al. (2013) showed that hydration of GCL causes swelling in bentonite, resulting in stretching of needle-punched fibres and changing the failure mechanism from fibre pull out to fibre rupture. Feng et al. (2020) studied the effect of displacement rate and normal stresses on the internal strength response of GCL specimens subjected to hydration. Fox et al. (1998) highlighted the effect of bentonite hydration on the internal shear strength of different types of GCLs. Reinforced products showed small decrease in peak and residual shear strengths with decrease in displacement rate. Literature suggests significant variation in peak interface shear strength for soil-needle punched GCL interfaces, depending on the soil type and test method (Chiu and Fox, 2004). Moderate to no post-peak strength reduction is reported for shear tests on dry sand-needle punched GCL and variety of other soil-needle punched GCL interfaces (Feki et al., 1997; Chiu and Fox, 2004). The studies with hydrated GCL specimens indicated that the residual shear strength of hydrated GCLs can only be improved by increasing the shear strength of hydrated bentonite (Fox and Stark, 2015).

The needle-punched reinforcing fibres of GCL are continuously subjected to shear stresses due to the gravitational weight of the overlying waste mass. As explained earlier, site conditions impose repeated shearing conditions on the GCLs. The reinforcing fibres of the GCL must sustain the cycles of tension and release, imposed by the shearing cycles. Polymer degradation and long-term polymer creep under imposed shear stresses are other factors that deteriorate the long-term performance of GCLs (Koerner et al., 2001; Zanzinger and Alexiew, 2000). Most of the studies available in literature on GCLs are limited to short term strength assessment. The long-term testing and performance of GCLs have not been investigated by many. It is very important to understand the performance of GCLs under repeated shearing conditions, at a macro level to understand the overall response and at micro level to investigate the mechanisms at fibre level. In this context, the current study presents results from repeated shear tests on sand-GCL interfaces to bring out the variations in the shear strength of these interfaces under repeated shearing cycles. The interface shear mechanisms and

progressive deterioration of the GCL specimens with shearing cycles were evaluated through high resolution digital image analysis of the tested GCL specimens. A natural river sand (RS) and a quarry manufactured sand (MS) of identical gradation and different particle shape were used in the experiments to investigate the effects of particle shape on the performance of the interfaces under repeated shearing. Results of the experimental investigations and microscopic image analysis of GCL-sand interfaces are analysed to draw some important conclusions on the performance of these sands and the GCL under repeated shearing conditions of the field.

## **2. Materials**

### **2.1 Geosynthetic Clay Liner (GCL)**

A commercial GCL called Macline GCL W was used in this study. The structure of this GCL consists of three layers, a layer of sodium bentonite containing 70% montmorillonite encapsulated between an upper nonwoven geotextile layer and a bottom woven geotextile layer, both made from polypropylene. The GCL is reinforced with needle punched fibres. The bentonite layer has water absorption capacity more than 650% and free swelling index of 24 ml/mg. The physical and engineering properties of GCL are presented in Table 1.

### **2.2 Sands**

A natural river sand (RS) and a quarry manufactured sand (MS) were used in this study. The gradations of these sands in their original state are presented in Figure 1. As per the Unified Soil Classification System (USCS), the river sand and the manufactured sand in their original composition were classified as poorly graded sand (SP) and well-graded sand (SW), respectively. To maintain identical gradation for these two sands in experiments, the size fractions of particles in both the sands are proportioned, to reach a gradation (target gradation) which lies between the original gradations of these two sands, as shown in Figure 1. The proportioned sands had identical gradation but different particle shapes. With this exercise, effects of particle size were eliminated in the tests, and comparisons were made only based on the particle shape. Table 2 presents the physical properties of the original and proportioned sands. High relative density of sand was maintained in all tests to simulate a compacted subgrade in the field. This ensured comparable void ratios in both the sands, as seen in Table 2. Thus, the variation in interface shear strength from shear tests on these specimens under identical interfacing and shearing conditions can mainly be attributed to the morphological characteristics of sands, as suggested by the studies of Santamarina and Cho (2001). The angle of internal friction of MS and RS at target gradation was determined as  $47^\circ$  and  $44^\circ$  from direct shear tests at 80% relative density.

Microscopic images of RS and MS particles show the differences in their particle shape (Figure 2). Average 3D shape parameters of the sand grains of both the types were determined through computational algorithms developed in MATLAB based on the *region properties* function using the Image processing tool box, applied to the microscopic images of sand particles (Pillai and Latha, 2022). Shape parameters were quantified by averaging the values of shape parameters of 200 individual particles of each type (MS and RS) from size fractions retained on sieves of 1.18 mm, 0.6 mm, 0.3 mm, 0.15 mm and 0.075mm sizes. The definitions, formulae and parametric descriptions along with the computed average values of sphericity, roundness, roughness, convexity, aspect ratio and elongation for the MS and RS particles are given in Table 3. The sphericity and roundness of particles represent rounded corners and near-spherical shape. Sphericity value of 1 represents the shape of a perfect sphere and values closer to 1 represent overall shape of the particle closer to a sphere. Roundness value of 1 represents perfectly rounded corners of the particles. Sphericity values are 0.78 and 0.84 for MS and RS, respectively, indicating that the shape of RS particles is more spherical compared to MS particles. Roundness of the MS particles is 0.39, which is slightly lower compared to the roundness of the RS particles, which is 0.42. Hence RS particles have relatively rounded corners compared to MS particles. Convexity values indicate the compactness of the particle shape, a value of 1 representing the most compact form. Irregularity in the form results in lower convexity values. RS particles have a convexity value of 0.87, indicating their regular form compared to MS particles having relatively lower convexity value of 0.78. Roughness gives an indication of surface asperities. Higher roughness values indicate irregular profile as shown by the MS particles. Normalized roughness values listed in Table 3 show that MS particles have twice the roughness compared to RS particles. Further, the elongation of particle shape is also a measure of shape proportioning of the particles, lower the elongation, more proportionate the shape. MS particles have higher elongation value of 0.34 compared to RS particles with elongation value of 0.22, indicating that MS particles are more elongated and irregular compared to RS particles. Hence, the irregular, less spherical and rough exterior of MS particles interact with fibres, resulting in increased frictional contact and improved resistance at interfaces.

### **3. Interface shear tests**

#### ***3.1 Description of the test setup***

A direct shear test setup modified to carry out interface shear tests on sand-geosynthetic interfaces with digital data acquisition facility was used in this study (Vangla and Latha, 2014; 2015). The bottom half of the conventional shear box was replaced with a square steel plate of dimension 180 mm × 180 mm, to which the GCL specimens were bolted with fastening steel plates to avoid sagging of the specimen during shearing. The shear box of dimensions 100 mm × 100 mm was filled with sand at the required density. The connections were checked after each shear cycle to ensure that they were intact. The rigid steel plate at the bottom and the rigid bolt connections used to fasten the GCL to the steel plate ensure that no sagging takes place in GCL specimens. A load cell was used to record the shear force at the interface and displacement of the GCL layer was measured using a linear variable differential transformer (LVDT). The interface shear test setup was fabricated as per ASTM D6243. Figure 3 shows a photograph of the interface shear test setup with GCL specimen fixed to the bottom plate.

#### ***3.2 Sample preparation***

For dry tests, GCL specimens of 180 mm × 180 mm were cut from the roll and bolted to the bottom steel plate of the interface shear setup. The GCL was fixed in a way that the nonwoven geotextile side of the GCL forms the interfacing surface. The shearing box was positioned over the GCL and held securely in that position using the holder and shaft arrangement. The relative density of the sand was maintained at 80% in all interface shear tests. The quantity of sand needed to fill the shearing box at this relative density was computed from the maximum and minimum unit weights of the sand and the dimensions of the box. Sand was filled in the shear box in three lifts of equal height, each lift lightly hand compacted using a small metal rod with enlarged base, to maintain the required density. For wet tests, GCL specimens were placed in a shallow pan and submerged in water under free swell condition before they were transferred to the shear box. This ensures uniform hydration of the GCL specimen, as suggested by Fox et. al., (1998). Unlike adhesive and stitch-bonded GCLs which need the application of normal stress for minimizing non-uniform swelling, needle-punched GCLs do not need any normal stress because of the in-plane transmissivity of nonwoven geotextile and the additional confinement provided by the reinforcing fibres (Fox et al., 1998). The specimens were submerged in water for 72 hours to achieve final water content and attain equilibrium condition based on the water content analysis of GCL specimens. The time required for reaching equilibrium water content in GCL under free swell conditions was

obtained prior to the interface shear tests. For this purpose, multiple GCL specimens were soaked in water in different containers and the water contents at different hydration times were recorded using a soil moisture sensor, namely CS655 Water content reflectometer. Results showed that GCL specimens attained equilibrium water content in 72 hours. This is confirmed through repeated tests, as shown in Figure 4.

To distinguish between MS and RS particles in experiments and to quantify the surface changes and particle entrapment on to the GCL specimens, MS particles were colored in red and RS particles were colored in green in experiments conducted under dry conditions. These colors were chosen to maintain a clear contrast between the sand particles and the fibres of the GCL. Food colors in the gel form were used for coloring. Since coloring agents like paints or powders could alter the surface roughness of particles and the gradation of sand, coloring gels were used to apply a thin uniform coat of color to the particles. The choice of food color is ideal in this scenario as it helped to maintain the original texture of particles. Sands were mixed with appropriate colors along with a little amount of water and oven dried. To ensure that the coloring does not affect the results, trial tests were conducted with original MS and colored MS at normal stresses of 100 kPa and 60 kPa. Figure 5 shows the stress-strain response for both the sands. The plot shows almost identical responses, confirming that the thin color coat used in this study does not affect the results. Figure 6a and 6b, respectively show red colored MS and green colored RS filled in shear box prior to testing and the surface of GCL after a typical test. To perform the tests under wet conditions, the sand was mixed with water to attain 18% water content, which is the saturation water content for both RS and MS. This was done to ensure equilibrium condition at the interface formed by the fully hydrated GCL and wet sand without transfer of moisture content. The fully hydrated GCL specimens were fixed to the steel platform and wet sand was filled in the shear box placed on top of it. The specific normal stress was applied and the shear tests were carried out without any time lag, to minimize the variation in moisture content of sand and GCL specimens. While the dry condition represents the highest possible interface strength, the fully hydrated condition represents the worst-case scenario of low shear strength, both these cases giving the boundaries for the interface shear strength to be expected in these interfaces. Sand was not colored in wet tests because the color is water soluble and there is a possibility of pores getting clogged with the color.

### **3.3 Interface direct shear tests of repeated load cycles**

The objective of these tests is to understand the variation in the performance of GCL-sand interfaces under repeated shearing conditions. For this purpose, specimens of sands interfacing with the nonwoven side of the GCL were subjected to repeated shearing under a specific normal load. Tests were conducted at normal stresses of 30 kPa, 60 kPa and 100 kPa, applied through a lever arm mechanism. This selected range of normal stresses represents the typical overburden stress on the capping and the baseliner of a landfill of moderate height. The interfaces were subjected to shearing at a constant rate of shear of 1.15 mm/min until the experimental limit of horizontal displacement was reached. This is within the possibilities of the experimental setup and close to the shear rate of 1 mm/min suggested by ASTM D6243 for interface shear tests on GCLs. Shear stress is computed from the horizontal load utilized for shearing the sample measured through a load cell connected to the box in horizontal direction and the contact area of the sand and the GCL layer. Once the test is complete, the shear box is brought back to the zero-displacement point, upper box with sand is removed from the setup, leaving the GCL fixed to the base plate. The same sample of sand is reconstituted in the upper box for the repeated shear test, with the sheared GCL interfacing with the sand. The repeated shear test was conducted under same normal stress as the original test till the limiting value of displacement was reached. This process was continued for eight shearing cycles with the same GCL layer. For wet tests, there is no time lapse between the mixing, filling and testing of the sand, which ensured that there is no loss of moisture. The water content of the tested sand was measured after each cycle to ensure that it was maintained close to 18%. Images of GCL were taken after each shearing cycle, to establish the surface changes with repeated shearing. These repeated shear tests were carried out for both types of sands (MS and RS) at all three normal stresses. In this paper, NGCL-MS and NGCL-RS refer to nonwoven geotextile-manufactured sand and nonwoven geotextile-river sand interfaces, respectively.

### **4. Results and discussions**

When interface shear test is conducted on a virgin GCL specimen, the results represent the shear strength mobilization at the interface immediately after the construction of the landfill. Over the time, the mobilized shear strength will change due to several factors, most important of them being the continuous shearing of the interfaces due to gentle slopes or periodic relative movement between the subgrade or cover soil and the GCL layer due to earthquake like scenarios. For obtaining the shear strength of the interfaces subjected to repeated shearing cycles, repeated shear tests were carried out in this study. While the first test represents the shearing of soil layer on a virgin GCL layer, the subsequent tests represent the repeated shearing on already stressed GCL

layer and corresponding shear strength mobilization of sand-GCL interfaces. Results from various interface tests carried out in this study are presented and discussed in the following sections.

#### ***4.1 Stress-strain response for repeated interface shearing tests***

Figure 7 shows the variation in the shear stress with horizontal displacement with repeated cycles for the NGCL-MS interfaces in dry and wet conditions at different normal stresses. For the first load cycle, the shear stress increased gradually with the increase in displacement at all normal stresses and for both dry and hydrated conditions. With the subsequent load cycles, the shear stress-displacement response was steeper compared to the first load cycle and the peak shear stress was attained at a lower displacement. Moreover, the peak shear stress reduced with hydration. The variation in peak shear stress with increase in load cycles and their relation to the hydration are not straightforward and observed to be dependent on several factors, which will be explained subsequently. Figure 8 shows the shear stress – displacement response of NGCL-RS interface for different load cycles under dry and wet conditions, at different normal stresses. The response of NGCL-RS interfaces is qualitatively similar to that of the NGCL-MS interfaces, except that the drop in peak shear stress with hydration is more significant for RS.

Variation of peak shear stress with number of repeated shear cycles for NGCL-MS and NGCL-RS are shown in Figure 9 and Figure 10, respectively. For the dry tests, it is observed that the peak shear stress decreased during the initial repeated cycles and then increased to reach a peak value in 4<sup>th</sup> or 5<sup>th</sup> cycle and started to slightly decrease then on. However, for wet tests, the trend is not consistent, except that the peak shear stress continuously decreased after the 4<sup>th</sup> cycle. Displacement at peak shear stress was 8–25 mm for both the interfaces in the first cycle and it decreased to 3–10 mm after 4 shearing cycles. As compared from Figure 9 and Figure 10, effects of hydration are seen to be more pronounced at higher normal stresses, especially for higher number of load cycles, because of higher bentonite extrusion. These effects are significant for RS interfaces compared to MS interfaces. To understand the reasons for the variations in shear resistance with number of cycles and with hydration, the images of tested GCL specimens before the test and after each shearing cycle were analysed.

## *4.2 Image analysis*

To monitor and understand the changes in the surface of GCL specimens after each shearing cycle and correlate them to the shearing resistance measured in interface shear tests, the images of virgin GCL specimen and tested GCL specimens after each shearing cycle were captured using Canon EOS 200D digital SLR camera. A fibre optic illuminator was used to maintain uniform light intensity while capturing the images. The images were analyzed using MATLAB R2021a to assess the surface changes to GCL specimens.

### *4.2.1 Key steps in image analysis*

Figure 11 shows the key steps involved in processing the image of the virgin GCL surface. The original image captured through camera was converted into a greyscale image through image processing toolbox in MATLAB. In the next step, multi-level thresholding technique was used to segment the image into fibres and voids, based on the intensity values of pixels. In the thresholded image, dark blue color represents voids and all other colors (cyan, yellow and green) represent fibres of GCL. These different colors of fibres represent variations in their surface reflectivity as the light was projected onto them, which can be seen in the original image. In the next step, binary image was constructed from the thresholded image, considering the fibres with all pixel intensities and voids. Inversion of binary image clearly shows the void structure in white color and fibres in the black background.

Figure 12 shows the key steps in image processing of a tested GCL surface. The tested GCL surfaces had sand particles entrapped in the voids of nonwoven geotextile. For description of image processing, the image of a typical GCL specimen after a dry interface test with MS was taken. The original image has a single entrapped MS particle in focus while other entrapped MS particles are seen as red spots embedded in the voids of lower layers of nonwoven fibre structure. Most of the voids are filled with sand particles, either on the surface or at the inner layers, as seen from the image. From the original image, greyscale image and thresholded image were obtained as discussed for the case of virgin GCL specimen. In the thresholded image, dark blue color represents sand particles and all other colors (cyan, yellow, and green) represent fibres of GCL with different reflectance values. If some voids were present, their area is insignificant and hence neglected in the present study. The thresholded image was converted to a binary image in the next step and inverted, to see the entrapped sand particle clearly. The inverted image was used to quantify the percentage area of entrapped sand particles on the GCL specimen.

#### 4.2.2 Image analysis of NGCL-sand interfaces after each shearing cycle

The shear area of tested GCL surfaces had dimensions of 120 mm × 100 mm. For carrying out image analysis, the shearing area was divided into 30 squares, each of size 20 mm × 20 mm. Each square was analyzed separately to get better resolution images. The image of each individual square was captured using a Canon EOS 200D Digital SLR camera and analyzed for entrapped sand particles, following the steps discussed in the previous section.

Original and binary images of GCL specimens of scan area of 20 mm × 20 mm after the dry repeated interface shear tests with MS are shown in Figure 13. GCL surfaces after each shearing cycle were analyzed. However, the images of these surfaces after 1<sup>st</sup>, 4<sup>th</sup> and 8<sup>th</sup> shearing cycles are presented in Figure 13 for understanding the progressive changes with repeated cycles. Similarly, original and binary images of GCL specimens after the dry tests with RS are presented in Figure 14. The white dots in the binary images of each cycle indicate the entrapped sand within the fibres of nonwoven GCL surface. As seen from Figure 13 and Figure 14, the density of white spots progressively increased with repeated shearing cycles. The images of tested GCL surface under wet conditions are presented in Figure 15 and Figure 16. As seen from the images, the entire surface of GCL is covered with sand particles under hydrated conditions, forming lumps towards the last cycle. The percentage area of entrapped sand within the sheared area of GCL was computed from the binary images, using the region properties function in MATLAB 2021a.

#### 4.5 Quantification of entrapped sand particles

The images of sheared GCL surfaces obtained with the high-resolution camera allowed the examination of the interface after each shearing cycle. The binary images of sheared GCL surfaces after each cycle were analyzed in MATLAB and the percentage of entrapped sand represented by white spots in the image, as explained earlier, was quantified through *region properties* function. Percentage area of entrapped sand particles at the end of each shearing cycle for NGCL-MS and NGCL-RS interfaces tested under dry and wet conditions are presented in Table 4. These values correspond to the total entrapped sand, obtained by adding up the values computed for all 30 square segments of the image. As observed from Table 4, entrapment of sand particles increased with the increase in the number of load cycles. In dry tested conditions, as the entrapment of sand on GCL surface is increased, sand to sand friction will start contributing to the shear resistance developed at the interface. At the beginning of the test, the interaction between the sand and fibres of GCL is the only component of shear resistance at the interface. As the test progresses and with the number of repeated shearing cycles, sand

entrapment starts to play major role in the mobilization of shear resistance. To understand this further, peak shear stress measured in each shearing cycle is plotted along with the percentage area of entrapped sand in that cycle, in Figure 17 and Figure 18 for MS and RS, respectively.

As observed from Figure 17 and Figure 18, the peak shear stress decreased for the second and third cycles for MS and second cycle for RS and then it increased up to 4<sup>th</sup> or 5<sup>th</sup> shearing cycle and then decreased with further cycles at all normal stresses. If sand entrapment is the only factor that is governing the shear resistance, the peak shear stress should increase continuously. However, the variation in peak shear stress has three phases as shown in Figure 17 and Figure 18- initial decrease, increase up to 4<sup>th</sup>/5<sup>th</sup> cycle and decrease there on. This behavior can be explained through three mechanisms- stretching of reinforcing needle-punched fibres of GCL, sand entrapment and pullout and rupture of GCL fibres.

During the initial shearing cycles, repeated shearing causes stretching of reinforcing needle-punched fibres of GCL, causing reduction in interface shear resistance. Though the shearing resistance increases with the sand entrapment, the reduction due to the stretching of needle-punched fibres and related loss of tension in GCL are the main reasons for the overall decrease of shear resistance during the second and third shearing cycles. As explained by Koerner et al. (2001), when shear stresses are applied to the upper nonwoven geotextile of GCL, these stresses get transmitted to the woven geotextile through the internal reinforcing fibre structures, which will be subjected to tension. During the second shearing cycle, the fibres are already stretched due to tension and hence cannot provide the same support to the upper NGCL layer. This loss of tension in internal reinforcement causes reduction in the shearing resistance developed at the interface. Figure 19 shows a schematic representation of internal reinforcing fibres connecting the upper and carrier geotextile layers. Figure 19a shows the needle-punched reinforcing fibres in a virgin GCL, which are originally not sheared. Figure 19b shows the fibres in a sheared GCL, which are stretched after being subjected to tension during the application of shear force. During the initial repeated cycles, this loss is higher than the increase in shearing resistance due to sand entrapment because the percentage sand entrapment is less. With further cycles, the sand entrapment increases considerably, overcoming the loss of shearing resistance due to the stretching of internal reinforcing fibres, thus increasing the overall shearing resistance of the interface. After 4<sup>th</sup> or 5<sup>th</sup> shearing cycle, the sand particles entrapped on the surface of the GCL get pushed into the voids of the nonwoven geotextile, reducing the sand-to-sand friction at the interface and overall shearing resistance. This aspect can be clearly visualized through digital images of virgin GCL, GCL after 3<sup>rd</sup> and 5<sup>th</sup> shearing cycles at a normal stress of 30 kPa with MS interface

captured through Olympus SZX10 stereo microscope. Figure 20 shows the image of nonwoven surface of GCL before testing, captured at 40x magnification. The fibres in the GCL are clean with a web like structure consisting of voids. Figure 21 shows the image of GCL after 3<sup>rd</sup> shearing cycle with MS interface. Sand particle entrapment on the surface of the GCL is clearly seen in this image, with a single particle focused on the image to show the details. Figure 22 shows the image of GCL after 5<sup>th</sup> shearing cycle with MS interface. As observed, the fibres are completely colored in the image and the sand particles are pushed deeper into the voids of the nonwoven geotextile. The sand particles present on the surface are insignificant at this stage, confirming that sand to sand friction is not contributing to the shearing resistance at this stage, as seen from Figure 17 for MS and Figure 18 for RS.

Figure 23 and Figure 24 show typical images of GCL surfaces with MS and RS interfaces, respectively, after 8<sup>th</sup> shearing cycle. The marked regions of these images show the rupture of fibres in GCL. The images after 5<sup>th</sup> cycle shown earlier did not reveal any rupture of the fibres. The rupture happened after the peak shear resistance is reached. The decrease in shearing resistance after 5<sup>th</sup> cycle is due to two reasons – pushing of entrapped sand particles deeper into voids of the nonwoven geotextile, which reduced the sand-to-sand friction and rupture of fibres of nonwoven geotextile, which caused reduction in sand-fibre interlocking and sand entrapment.

In wet tests, the sand entrapment on the surface of the GCL is significantly higher than the entrapment in dry tests for both MS and RS interfaces. Peak shear stress measured in each shearing cycle for wet tests is plotted along with the percentage area of entrapped sand in that cycle, in Figure 25 and Figure 26 for MS and RS, respectively. As seen from these figures, sand entrapment is quicker in wet conditions and reached almost 100% at 4<sup>th</sup> cycle. This high percentage of entrapment must result in increased sand-sand friction at interfaces.

However, repeated shearing cycles result in stretching of the internal reinforcing fibres, in turn resulting in reduced interface shear strength. Further, in wet tests, the effect of lubricating water at the interface and the slimy surface formed at the interface by the extruded bentonite contribute to the reduction of interface shear strength. Figure 27 shows the microscopic images of GCL prior to shearing, which show a lubricating water film and the slimy layer of extruded bentonite seen on the nonwoven surface of the GCL. Since the sand entrapment and the slimy layer formation are not uniform across the GCL surface in wet tests, there is a randomness in the variation of shear strength during the initial loading cycles. However, after 4<sup>th</sup> cycle, the effects of sand entrapment are overcome by the effects of fibre stretching and bentonite extrusion, which resulted in continuous loss of shear strength with subsequent load cycles, as seen in Figure 25 and Figure 26.

Table 5 presents the peak interface friction ( $\phi_p$ ) and adhesion ( $a_p$ ) and residual interface friction ( $\phi_r$ ) and adhesion ( $a_r$ ) of NGCL-MS and NGCL-RS interfaces, after each shearing cycle, for both dry and wet tests. As observed from Table 4, the area of sand particle entrapment was less for NGCL-MS interfaces compared to NGCL-RS interfaces. However, from Table 5, it can be observed that NGCL-MS interfaces showed better peak and residual friction angles compared to NGCL-RS interfaces for all shearing cycles. The peak and residual adhesion values of both these interfaces are not too different for many cases. Overall, the shear strength of NGCL-MS interfaces is higher than NGCL-RS interfaces, which can be attributed to the particle shape. Since MS particles are more elongated and rougher, the sand-sand interaction provided higher interface shear resistance compared to more spherical and rounder particles of RS. For the dry tests, as seen from Table 5, the peak friction angle decreased from a value of  $40^\circ$  in the first cycle to a value of  $38^\circ$  in the eighth cycle for MS interfaces, which is about 4% decrease with eight repeated shear cycles. For RS interfaces, the decrease in peak friction angle is from  $39^\circ$  to  $36^\circ$ , which is about 7.4% decrease with eight repeated cycles. The peak interface adhesion reduced by about 29% from first cycle to eighth cycle for both MS and RS interfaces. However, in the hydrated conditions, the peak friction angle for NGCL-MS interface reduced from  $34^\circ$  in first cycle to  $30^\circ$  in eighth cycle, which is about 13% reduction. For NGCL-RS interface, the reduction in peak interface friction angle is almost 27% from first to eighth cycle. This is predominantly due to the presence of lubricating water at the interface. The adhesion values are observed to be generally higher for all interfaces in wet tests compared to dry tests due to the slimy bentonite layer at the interface, which sticks to the particles and binds them. Though MS particles were less entrapped and there is a higher possibility of MS particles damaging the fibres of nonwoven geotextile compared to RS particles, the peak shear resistance of NGCL-MS interfaces is higher compared to NGCL-RS interfaces. Further, the decrease in peak friction angle is much lower in NGCL-MS interfaces because of the particle shape effects leading to efficient interlocking and better shear resistance. Lower sphericity values of MS particles provide a larger contact area compared to RS particles. In addition to that, MS particles have rough surface texture, providing relatively higher frictional resistance at the interface. Conventionally, the interface shear strength used for the design of landfill covers and baseliners is from the single cycle shear test. Based on the observations from repeated shear tests, it is clear that repeated shearing cycles on GCL due to various reasons cause significant reduction in the interface shear resistance. Further, the peak shear resistance occurs comparatively at lower displacements with repeated cycles of shear up to 4<sup>th</sup> cycle after which the peak shear resistance occurred within 5-10 mm of displacement. For large displacement

conditions, the conventional approach of obtaining the design interface shear strength from a single cycle shear test will lead to overestimation of the shear strength of the interface, leading to failure. In such conditions, using interface shear strength obtained from repeated shear cycles will be a safer option. From the current study, the displacements corresponding to peak shear resistance were observed to be stable after 4 shearing cycles. Hence repeated shear tests up to a minimum of 7 shearing cycles are recommended for obtaining realistic interface shear strength values. For practical designs, residual interface shear strength parameters obtained after 7 load cycles can be used because the reduction in strength and reduction in displacement corresponding peak strength are both observed to be stable after 7<sup>th</sup> cycle. Further, the efficiency NGCL-MS interfaces over NGCL-RS interfaces in terms of higher interface shear strength and lesser degradation of shear strength with repeated cycles and hydration is evident from the experimental results. Hence manufactured sand can be an efficient alternative to the natural sand for subgrade and cover soil in the landfills.

The results presented in this paper are from a small direct shear setup, which has limitations on maximum displacement and normal stresses that can be applied. The repeated shear tests are designed to closely simulate the field conditions of GCLs subjected to repeated shearing to understand the mechanisms responsible for the variation of shear strength. The objective is to compute macroscopic interface shear strength at different shearing cycles through interface shear tests and relating them to microscopic surface changes through digital image analysis. There could be minor variations between the experimental and field conditions of repeated shear. However, some important mechanisms like stretching of internal reinforcing fibres, sand particle entrapment and intrusion and rupture of fibres at different cycles of shearing and their influence on the overall shearing resistance of GCL-sand interfaces are clearly brought out from the present study. The effects of creep and degradation are not considered in the present study.

## 5. Conclusions

Major conclusions drawn from the repeated shear tests on nonwoven side of the GCL (NGCL) interfacing with manufactured sand (MS) and river sand (RS) in dry and wet conditions and digital image analysis of tested GCL surfaces are as follows.

1. The variation of interface shear strength of GCL-sand surfaces with repeated load cycles is influenced significantly by many parameters, including sand entrapment, specimen hydration, stretching of internal reinforcing fibres and bentonite extrusion.

2. The interface shear stress response of NGCL-sand interfaces in dry and wet conditions provided the limits of variation of shear strength parameters for both NGCL-MS and NGCL-RS interfaces. The peak interface friction angle was  $40^\circ$  for NGCL-MS interface in the first cycle in dry test and it dropped to  $38^\circ$  in eighth cycle. For the wet tests, the reduction was more significant, from  $34^\circ$  in the first cycle to  $30^\circ$  in the eighth cycle. For NGCL-RS interface, the reduction of peak interface friction angle was  $39^\circ$  to  $36^\circ$  in dry tests and  $33^\circ$  to  $26.5^\circ$  in wet tests.
3. The change in shear resistance from single cycle shear to eight cycles of shear has three phases in dry tests. The first phase is governed by the stretching of internal reinforcing fibres of GCL, causing decrease in shear resistance. The second phase is controlled by the sand particle entrapment which increased the shear resistance due to, sand-sand friction. The third phase is governed by pushing of entrapped sand particles into the voids of the nonwoven geotextile, causing reduction in sand-sand friction and overall shear resistance at the interface.
4. The first phase lasted till 2<sup>nd</sup> or 3<sup>rd</sup> cycle, the second phase occurred between 3<sup>rd</sup> and 5<sup>th</sup> cycle and the third phase is seen beyond the 5<sup>th</sup> cycle of shearing for both the manufactured and river sand used in experiments.
5. The three phases of shear resistance in dry tests are explained through digital image analysis of virgin and tested GCL surfaces. The virgin GCL surface showed clean fibres with a web like structure with voids. The GCL tested after 3<sup>rd</sup> cycle showed sand particles entrapped on the surface. The GCL tested after 5<sup>th</sup> cycle showed sand particles intruded into the voids of the deeper layers of nonwoven geotextile.
6. Images of GCL at the end of eight cycles of shearing in dry tests showed fibre rupture at several locations, which is another reason for the reduction of shear resistance beyond five cycles of shearing.
7. In wet tests, the change in interface shear strength from first to eighth load cycle is governed by multiple parameters, most importantly, the lubrication effect due to hydration, random entrapment of sand, non-uniform extrusion of bentonite and internal fibre stretching. Under the combined effect of all these parameters, the variation on shear strength is random in the initial cycles of loading and beyond 4<sup>th</sup> cycle, it showed continuous reduction.

8. The percentage area of sand particle entrapment computed through MATLAB algorithm is correlated to the variation in shearing resistance. Though the sand particle entrapment was higher in case of river sand (RS), interfaces with manufactured sand (MS) showed higher shear resistance at all cycles due to larger contact area at the interface resulting from the lower sphericity of their particles.
9. The interface adhesion values in all interfaces are in general higher for wet tests compared to dry tests because of the stickiness induced by extruded bentonite.
10. The peak friction angle decreased by 4% for MS interfaces, and 7.4% for RS interfaces after eight repeated shear cycles. The peak interface adhesion reduced by about 29% in eight shear cycles for both MS and RS interfaces. Hence manufactured sand with particles of lesser sphericity and roundness provides efficient interfaces with GCLs compared to river sand with rounded particles.
11. The displacement corresponding to peak shear resistance decreased with repeated shearing cycles until 4<sup>th</sup> cycle. Displacement at peak shear stress was 8–25 mm for both the interfaces in the first cycle and it decreased to 3-10 mm after 4 shearing cycles.

#### **Acknowledgements**

The GCLs used in the present research work are provided by M/s Maccaferri Environmental Solutions Pvt. Ltd. The digital microscope used for the image analysis was procured through the SERB POWER Fellowship of the corresponding author. Authors are grateful to these agencies for their support.

#### **List of notations**

$\phi_{pd}$	interface friction at peak shear stress in dry condition, in degrees
$a_{pd}$	interface adhesion at peak shear stress in dry condition, in kPa
$\phi_{rd}$	interface friction at residual shear stress in dry condition, in degrees
$a_{rd}$	interface adhesion at residual shear stress in dry condition, in kPa
$\phi_{ph}$	interface friction at peak shear stress in hydrated condition, in degrees
$a_{ph}$	interface adhesion at peak shear stress in hydrated condition, in kPa
$\phi_{rh}$	interface friction at residual shear stress in hydrated condition, in degrees
$a_{rh}$	interface adhesion at residual shear stress in hydrated condition, in kPa

#### **List of abbreviations**

GCL	Geosynthetic Clay Liner
LVDT	Linear Variable Differential Transformer
MS	Manufactured Sand
NGCL	Nonwoven side of the GCL

RS	River Sand
SP	Poorly graded Sand
SW	Well-graded Sand
USCS	Unified Soil Classification System

#### References

- ASTM D6243. (2020). Standard Test Method for Determining the Internal and Interface Shear Strength of Geosynthetic Clay Liner by the Direct Shear Method. ASTM International, West Conshohocken, PA
- Bacas, B. M., Blanco-Fernandez, E., & Cañizal, J. (2013). Comparison of the adhesion and shear tensile strength of needle-punched GCLs. *Geotextiles and Geomembranes*, 41, 17-25.
- Bergado, D.T., Ramana, G.V., & Sia, H.I. (2006). Evaluation of interface shear strength of composite liner system and stability analysis for a landfill lining system in Thailand. *Geotextiles and Geomembranes*, 24(6): 371–393.
- Blight, G. E. (2007). Failures during construction of a landfill lining: a case analysis. *Waste management & research*, 25, No. 4, 327-333.
- Bonaparte, R., Bachus, R. C. & Gross, B A. (2020) Geotechnical stability of waste fills: Lessons learned and continuing challenges. *Journal of Geotechnical and Geoenvironmental Engineering*, 146, No. 11, 05020010.
- Bouazza, A. (2002). Geosynthetic clay liners. *Geotextiles and Geomembranes*, 20, 3-17.
- Chang, J. Y., Feng, S. J., Zheng, Q. T., & Shen, Y. (2021). Cyclic shear behavior of GMB/GCL composite liner. *Geotextiles and Geomembranes*, 49, No. 3, 593-603.
- Chiu, P. & Fox, P. J. (2004). Internal and interface shear strengths of unreinforced and needle-punched geosynthetic clay liners. *Geosynthetics International*, 11, No. 3, 176–199.
- Eid, H.T. (2011). Shear strength of geosynthetic composite systems for design of landfill liner and cover slopes. *Geotextiles and Geomembranes*, 29, No. 3, 335–344.
- Feki, N., Garcin, P., Faure, Y. H., Gourc, J. P. & Berroir, G. (1997). Shear strength of geosynthetic clay liner systems. *Proceedings of Geosynthetics '97*, IFAI, Long Beach, California, USA, Vol. 2. 899–912.
- Feng, S. J., Chang, J. Y., Chen, H. X., Shen, Y., & Shi, J. L. (2020). Shear strength and failure mechanism of needle-punched geosynthetic clay liner. *Geotextiles and Geomembranes*, 48, No. 6, 962-972.

- Fox, P. J., Scheithe, J. R., & Rowland, M. G. (1997). Shear strength of reinforced geosynthetic clay liner (Discussion)." *Journal of Geotechnical and Geoenvironmental Engineering, ASCE*, 124, No. 12, 1178-1179.
- Fox, P. J., Rowland, M. G., & Scheithe, J. R. (1998). Internal shear strength of three geosynthetic clay liners. *Journal of Geotechnical and Geoenvironmental Engineering*, 124, No. 10, 933-944.
- Fox, P. J., & Stark, T. D. (2015). State-of-the-art report: GCL shear strength and its measurement—ten-year update. *Geosynthetics International*, 22, No. 1, 3-47
- Fox, P. J., Sura, J. M., & Nye, C. J. (2015). Dynamic shear strength of a needle-punched GCL for monotonic loading. *Journal of Geotechnical and Geoenvironmental Engineering*, 141, No. 7, 04015025.
- Gilbert, R. B., Fernandez, F. F., & Horsfield, D. (1996). Shear Strength of a Reinforced Clay Liner. *Journal of Geotechnical and Geoenvironmental Engineering, ASCE*, 122, No. 4, 259-266.
- Hou, J., Li, H., & Liu, L. (2018). An experimental study on microstructure of leachate-polluted stabilized clay. *Environmental Earth Sciences*, 77, No. 18, 1-10.
- Koerner, R. M., & Soong, T. Y. (2000). Leachate in landfills: the stability issues. *Geotextiles and Geomembranes*, 18, No. 5, 293-309.
- Koerner, R. M., Soong, T. Y., Koerner, G. R., & Gontar, A. (2001). Creep testing and data extrapolation of reinforced GCLs. *Geotextiles and Geomembranes*, 19, No. 7, 413-425.
- Lupini, J. F., Skinner, A. E., & Vaughan, P. R. (1981). The drained residual strength of cohesive soils." *Geotechnique*, 31, No. 2, 181-213.
- McCartney, J. S., Zornberg, J. G., & Swan Jr, R. H. (2009). Analysis of a large database of GCL-geomembrane interface shear strength results. *Journal of Geotechnical and Geoenvironmental Engineering*, 135(2), 209-223.
- Olsta, J. T., & Swan Jr, R. H. (2001). Internal shear strength of a geosynthetic clay liner at high normal loads. *Proceedings of Tailings and Mine Wastes 2001*, Fort Collins, CO, 197-200.
- Pitanga, H. N., Gourc, J. P., & Vilar, O. M. (2009). Interface shear strength of geosynthetics: evaluation and analysis of inclined plane tests. *Geotextiles and Geomembranes*, 27, No. 6, 435-446.
- Pillai, Anjali G., and Madhavi Latha Gali. "Role of particle shape on the shear strength of sand-GCL interfaces under dry and wet conditions." *Geotextiles and Geomembranes* 50, no. 2 (2022): 262-281.

- Rowe, R. K., & Orsini, C. (2003). Effect of GCL and subgrade type on internal erosion in GCLs under high gradients. *Geotextiles and Geomembranes*, 21, No. 1, 1-24.
- Booker, J. R., Brachman, R., Quigley, R. M., & Rowe, R. K. (2004). *Barrier systems for waste disposal facilities*. CRC Press, London, UK.
- Reyes Ramirez, R., & Gourc, J. P. (2003). Use of the inclined plane test in measuring geosynthetic interface friction relationship. *Geosynthetics International*, 10, No. 5, 165-175.
- Santamarina, J. C., & Cho, G. C. (2001). Determination of critical state parameters in sandy soils—simple procedure. *Geotechnical testing journal*, 24, No. 2, 185-192.
- Siebken, J. R., Swan, R. H., & Yuan, Z. (1997). Short-term and creep shear characteristics of a needlepunched thermally locked geosynthetic clay liner. In *Testing and Acceptance Criteria for Geosynthetic Clay Liners*. ASTM International.
- Stark, T. D., Arellano, D., Evans, W. D., Wilson, V. L., & Gonda, J. M. (1998). Unreinforced geosynthetic clay liner case history. *Geosynthetics International*, 5, No. 5, 521-544.
- Stark, T. D., Newman, E. J., & Aust, R. L. (2008). Back-analysis of a PVC geomembrane-lined pond failure. *Geosynthetics International*, 15, No. 4, 258-268.
- Stoltz, G., & Herval, A. (2014, September). Assessing interface friction angles of geosynthetics by comparing two loading methods. In *10th International Conference on Geosynthetics* (p. 7).
- Tano, F., Olivier, F., Touze-Foltz, N., & Dias, D. (2015). State-of-the-art of piggy-back landfills worldwide: comparison of containment barrier technical designs and performance analysis in terms of geosynthetics stability. *Geosynthetics 2015, Portland, USA*, 11.
- Touze-Foltz, N., Barroso, M., & Cartaud, F. (2006). Experimental investigation of flow rates through composite liners at the metric scale. In *Geosynthetics, Volumes 1-4. Proceedings of the 8th International Conference on Geosynthetics (8ICG)*, Yokohama, Japan, 305-308. Millpress Science Publishers.
- Vangla, P., & Gali, M. L. (2014). Image-segmentation technique to analyze deformation profiles in different direct shear tests. *Geotechnical Testing Journal*, 37, No. 5, 828-839.
- Vangla, P., & Latha, G. M. (2015). Influence of particle size on the friction and interfacial shear strength of sands of similar morphology. *International Journal of Geosynthetics and Ground Engineering*, 1, No.

Wu, W., Wang, X. T., & Aschauer, F. (2008). Investigation on failure of a geosynthetic lined reservoir.

*Geotextiles and Geomembranes*, 26, No. 4, 363-370.

Zanzinger, H. (2016). Contribution to the long-term shear strength of a needle punched GCL. *International Journal of Geosynthetics and Ground Engineering*, 2, No. 1, 8.

Zanzinger, H., & Alexiew, N. (2000). Prediction of long-term shear strength of geosynthetic clay liners with shear creep tests. In *Proceedings 2nd European Conference on Geosynthetics, Bologna.*, 2, 567-571.

Zornberg, J. G. (2009). Chapter 8: Internal and interface shear strength of geosynthetic clay liners. *Geosynthetic Clay Liners for Waste Containment Facilities*, 149-174

Table 1 Properties of GCL

Property	Value
Mass per unit area ( $\text{g/m}^2$ )	4300
Nominal thickness (mm)	6.0
Permeability (m/sec)	$5 \times 10^{-11}$
Tensile strength (longitudinal) (kN/m)	11.5
Average peel strength (N/m)	650

Table 2. Properties of sand

Property	Natural gradation		Target gradation	
	River sand (RS)	Manufactured sand (MS)	River sand (RS)	Manufactured sand (MS)
Gradation	Poorly graded	Well graded	Poorly graded	Poorly graded
Coefficient of curvature, $C_u$	4.375	9.374	5.8	5.8
Coefficient of curvature, $C_c$	0.55	1.41	1.12	1.12
Specific gravity	2.69	2.57	2.69	2.58
Maximum void ratio ( $e_{max}$ )	0.69	0.54	0.54	0.54
Minimum void ratio ( $e_{min}$ )	0.61	0.39	0.47	0.46

Table 3. Average shape parameters of sands

Shape parameter	Definition	Formula	Parametric description	River sand (RS)	Manufactured sand (MS)
Sphericity	Ratio of the diameter of the circle having an area equal to the largest projected area of the particle to the diameter of the smallest circle that circumscribes the projection Range – 0 to 1	$\frac{D}{D_{cir}}$	$D$ - diameter of the circle with same projected area as that of the particle; $D_{cir}$ - diameter of the smallest circumscribing circle of the particle.	0.8473	0.7859
Roundness	Measure for the smoothness of the particle boundary Range – 0 to 1	$\frac{\sum_{i=1}^N r_i / N}{R_{max}}$	$r$ - radius of the circle formed at corners of the projected area of particle; $N$ - number of identified corners of the projected area of the particle; $R_{max}$ - radius of the largest inscribed circle within the particle	0.4178	0.3906
Normalized Roughness	Computed as the difference between the raw profile and the smoothed profile of the particle, using conventional root mean square formula Range – Greater than 0	$\frac{\sqrt{\frac{1}{N} \sum_{i=1}^N (y_{ir} - y_{is})^2}}{L}$	$N$ - number of measurements $y_{ir}$ - $i^{\text{th}}$ coordinate of the raw profile $y_{is}$ - $i^{\text{th}}$ coordinate of the smoothed profile $L$ – length of particle	0.0012	0.0024
Convexity	Ratio of the projected area of the particle and the convex polygon formed along the outline of the particle, which is termed as the convex hull. Range – 0 to 1	$\frac{A(T)}{A(T) + B}$	$A(T)$ - projected area of the particle $B$ - area occupied by the convexity formed by the irregularity of the edge of the particle	0.8676	0.7858
Aspect ratio	Ratio can be computed as the ratio of the minimum Feret distance to the maximum Feret distance Range – 0 to 1	$\frac{X_{Fmin}}{X_{Fmax}}$	$X_{Fmin}$ – minimum Feret distance $X_{Fmax}$ – maximum Feret distance	0.7710	0.6535
Elongation	Measure of the proportion of the particle	$I-AR$	$AR$ - aspect ratio of the particle	0.2292	0.3465

Table 4 Area of entrapped sand after each load cycle for different interfaces

Interface	Test conditions	Normal stress (kPa)	Area of entrapped sand (%)							
			Load cycle							
			1	2	3	4	5	6	7	8
NGCL-MS	Dry	30	11.6	13.2	16.11	20.35	22.62	24.78	26.44	28.16
		60	12.89	15.23	18.52	22.49	24.36	25.89	27.91	30.10
		100	14.28	16.72	19.86	23.14	25.37	26.38	30.14	31.93
	Hydrated	30	48.56	58.36	79.59	88.29	96.23	98.59	98.94	99.12
		60	62.43	75.98	84.51	92.63	96.18	99.14	99.63	99.85
		100	70.53	89.23	93.56	97.29	98.16	99.13	99.85	100.00
NGCL-RS	Dry	30	14.21	17.39	20.37	23.62	25.54	27.19	28.77	30.48
		60	17.74	20.17	23.58	25.14	27.84	29.67	31.18	33.18
		100	20.37	22.49	24.33	26.47	27.96	29.41	32.83	34.56
	Hydrated	30	75.21	84.13	95.23	96.19	97.86	99.12	100.00	100.00
		60	85.24	92.67	95.83	98.45	99.25	99.53	100.00	100.00
		100	90.26	93.73	98.26	99.63	100.00	100.00	100.00	100.00

Table 5 Shear strength parameters

Load cycles	NGCL-MS								NGCL-RS							
	At peak shear stress				At residual shear stress				At peak shear stress				At residual shear stress			
	Dry		Hydrated		Dry		Hydrated		Dry		Hydrated		Dry		Hydrated	
	$\phi_p$	$a_p$	$\phi_{ph}$	$a_{ph}$	$\phi_r$	$a_r$	$\phi_{rh}$	$a_{rh}$	$\phi_p$	$a_p$	$\phi_{ph}$	$a_{ph}$	$\phi_r$	$a_r$	$\phi_{rh}$	$a_{rh}$
1	40.03	25.31	34.60	23.51	41.02	13.60	31.38	20.00	38.95	24.71	33.02	16.70	36.99	20.00	30.96	16.00
2	41.12	20.30	32.62	29.53	40.69	14.18	30.96	18.00	40.36	20.37	30.96	17.18	40.03	10.41	31.30	15.30
3	41.61	18.14	36.86	23.78	40.36	12.65	31.79	18.70	40.53	18.34	30.90	16.50	38.65	12.67	30.11	22.15
4	42.61	19.00	37.95	21.43	40.38	12.16	34.99	16.21	41.02	19.69	34.90	15.90	38.72	12.26	24.22	24.00
5	40.01	19.42	35.37	22.56	38.30	15.39	33.82	18.30	40.32	20.37	30.11	20.00	38.36	11.25	26.56	18.80
6	39.69	19.36	34.20	21.41	37.23	15.29	33.02	20.01	38.35	20.30	31.38	18.12	38.60	9.98	28.81	18.80
7	39.35	18.95	32.20	19.60	37.22	12.10	32.21	18.88	37.10	18.52	29.20	20.20	36.12	8.26	25.64	20.60
8	38.30	17.78	30.01	20.56	36.12	11.56	30.96	15.02	36.05	17.65	26.52	19.18	36.11	8.54	22.72	21.15

**Figure captions**

- Figure 1 The particle size distribution plots for river sand (RS) and manufactured sand (MS) and the chosen gradation (target).
- Figure 2 Microscopic image of sand particles obtained with Nikon 80i optical microscope (a). MS particles (b) RS particles.
- Figure 3 Photograph of the interface shear setup with GCL specimen
- Figure 4 Variation of GCL water content with hydration time
- Figure 5 Stress strain response of shear tests with plain and colored sand
- Figure 6 Colored sands in interface shear tests (a) MS (red) (b) RS (green)
- Figure 7 Shear stress – horizontal displacement plots with repeated load cycles for NGCL-MS interface at different normal stresses in dry and hydrated conditions
- Figure 8 Shear stress – horizontal displacement plots with repeated load cycles for NGCL-RS interface at different normal stresses in dry and hydrated conditions
- Figure 9 Variation of peak shear stress and displacement at peak shear stress for NGCL-MS interface under load cycles
- Figure 10 Variation of peak shear stress and displacement at peak shear stress for NGCL-RS interface under load cycles.
- Figure 11 Key steps in image processing of virgin GCL surface (Nonwoven side)
- Figure 12 Key steps in image processing of tested GCL surface
- Figure 13 Images of tested square segment of GCL surfaces after dry shear test with entrapped MS particles after 1<sup>st</sup>, 4<sup>th</sup> and 8<sup>th</sup> cycles of shearing at a normal stress of 30 kPa (a) Original images (b) Binary images
- Figure 14 Images of tested square segment of GCL surfaces after dry shear test with entrapped RS particles after 1<sup>st</sup>, 4<sup>th</sup> and 8<sup>th</sup> cycles of shearing at a normal stress of 30 kPa (a) Original images (b) Binary images
- Figure 15 Images of tested square segment of GCL surfaces after wet shear test with entrapped MS particles after 1<sup>st</sup>, 4<sup>th</sup> and 8<sup>th</sup> cycles of shearing at a normal stress of 30 kPa (a) Original images (b) Binary images
- Figure 16 Images of tested square segment of GCL surfaces after wet shear test with entrapped RS particles after 1<sup>st</sup>, 4<sup>th</sup> and 8<sup>th</sup> cycles of shearing at a normal stress of 30 kPa (a) Original images (b) Binary images
- Figure 17 Variation of peak shear stress and sand entrapment with load cycles for MS interfaces
- Figure 18 Variation of peak shear stress and sand entrapment with load cycles for RS interfaces
- Figure 19 Schematic representation of GCL (a) virgin GCL layer (b) sheared GCL layer
- Figure 20 Image of untested GCL specimen captured at 40x magnification by stereo microscope.

# Accepted manuscript doi: 10.1680/jgein.22.00352

---

Figure 21 Image of tested GCL specimen interfaced with MS particles captured at 32x magnification by stereo microscope

Figure 22 Image of tested NGCL-MS interface captured at 40x magnification by stereo microscope.

Figure 23 Typical images of tested GCL surfaces showing the pull-out and rupture of fibres NGCL-MS after 8<sup>th</sup> shearing cycle

Figure 24 Typical images of tested GCL surfaces showing the pull-out and rupture of fibres NGCL-RS after 8<sup>th</sup> shearing cycle

Figure 25 Variation of peak shear stress and sand entrapment with load cycles for MS interfaces

Figure 26 Variation of peak shear stress and sand entrapment with load cycles for RS interfaces

Figure 27 Images of GCL surface under hydrated condition (a) lubricating film of water seen prior to shear (b) Extrusion of bentonite on to the nonwoven surface of GCL

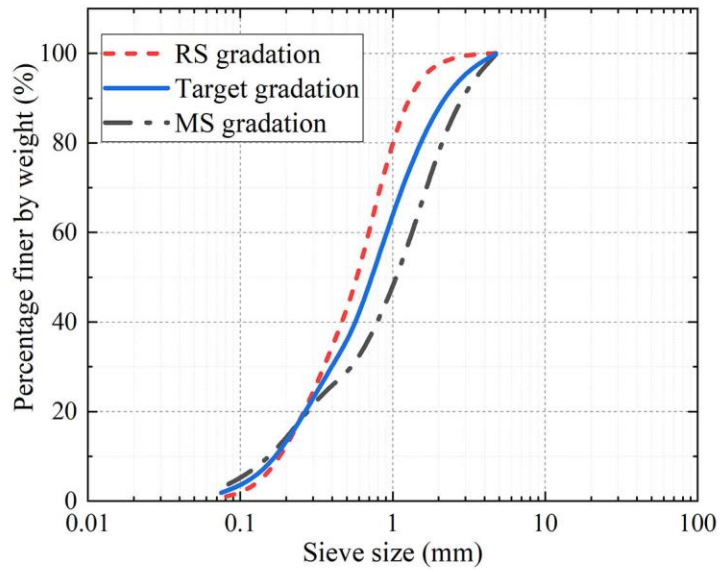


Figure 1

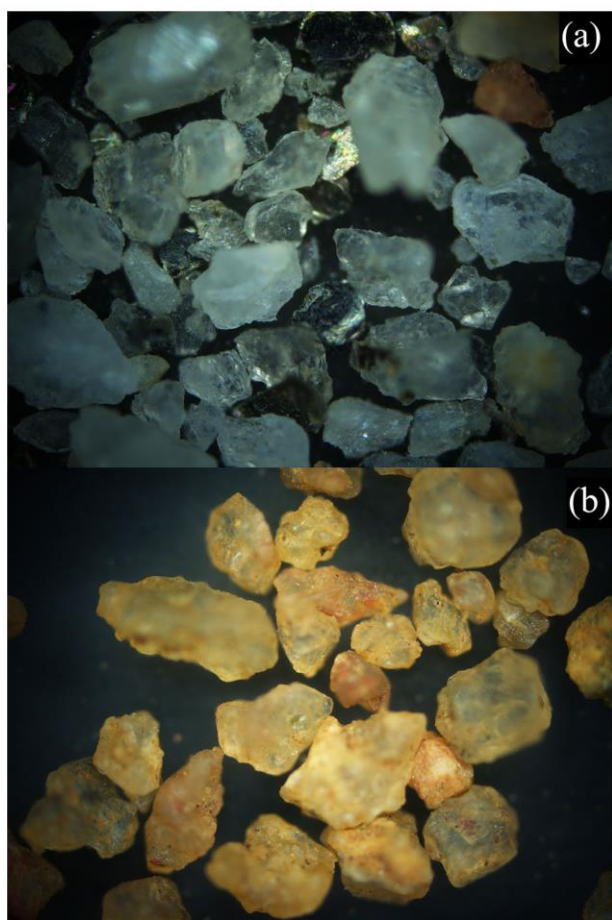


Figure 2

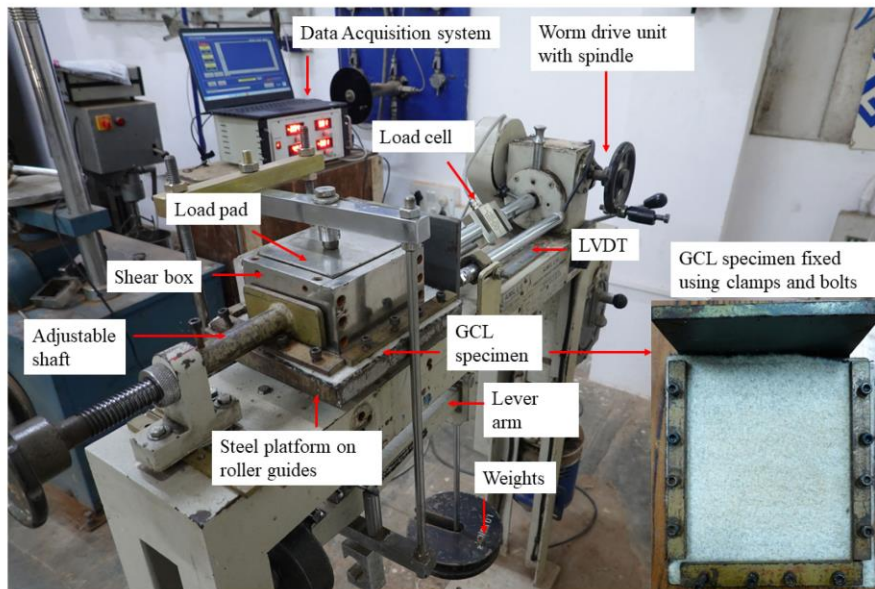


Figure 3

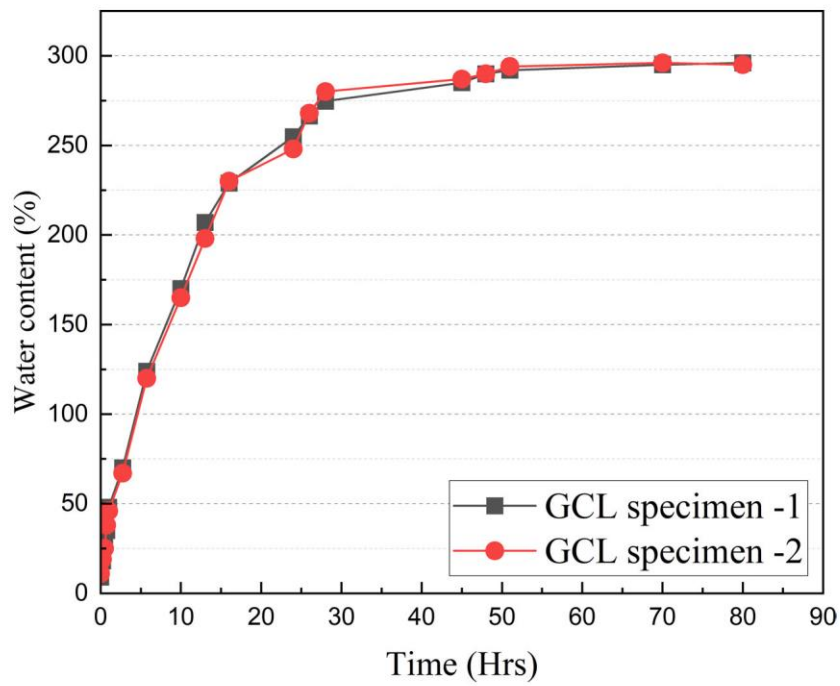


Figure 4

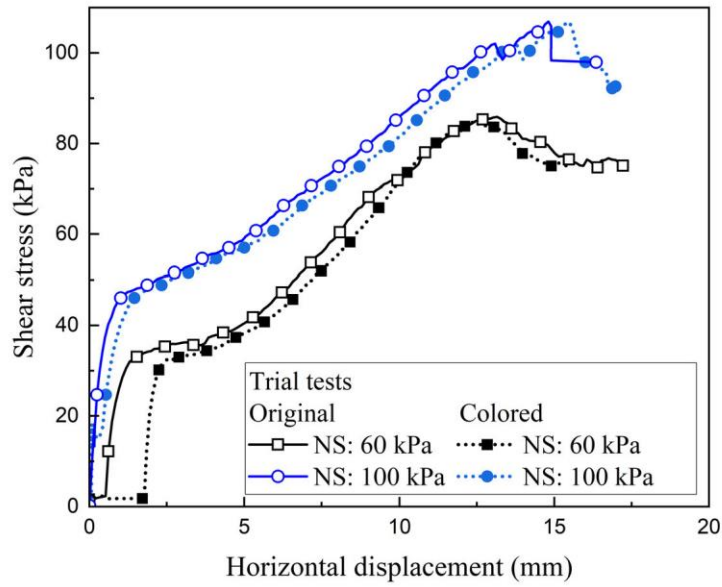


Figure 5

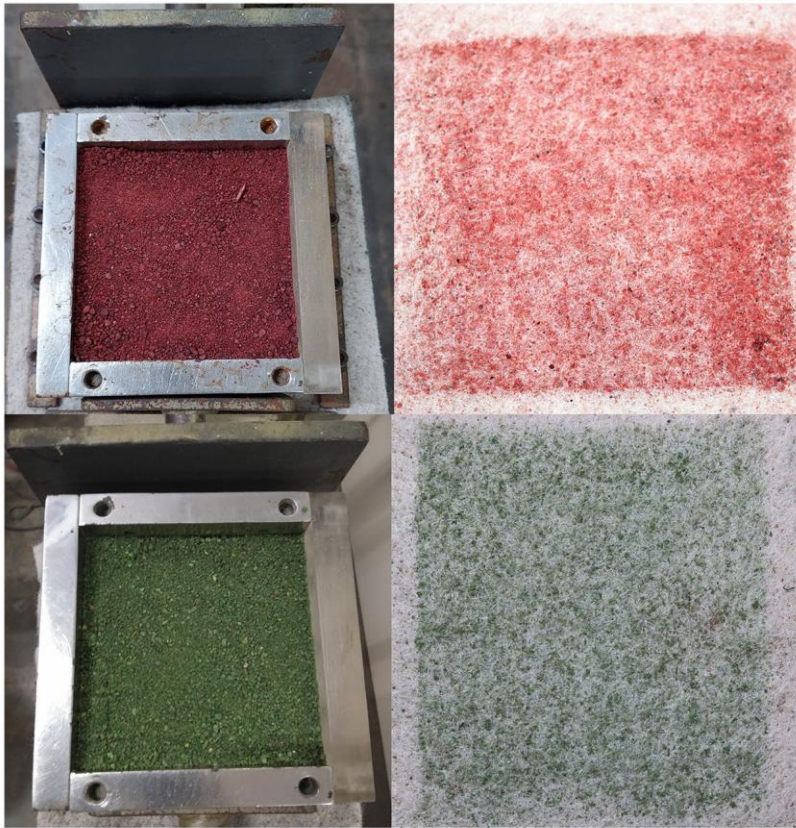


Figure 6

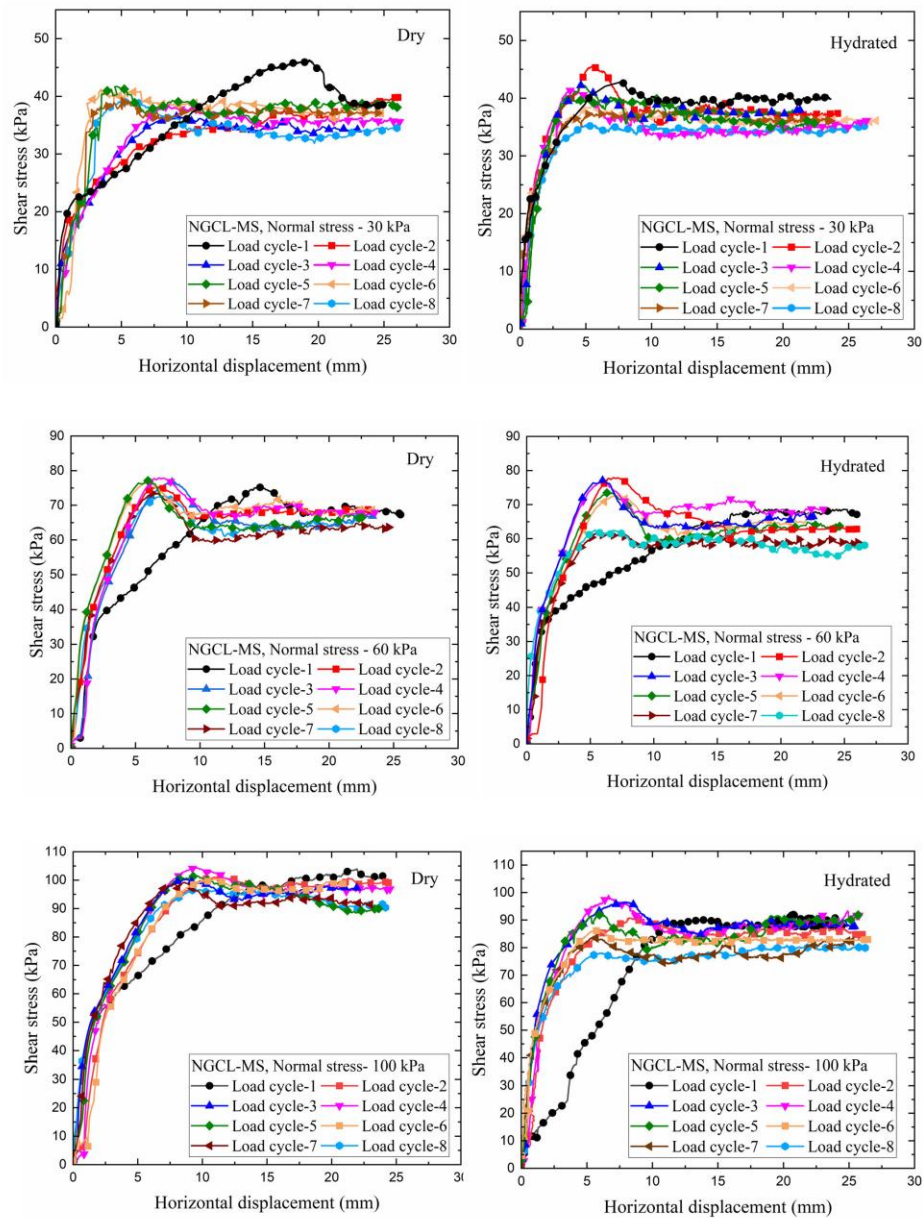


Figure 7

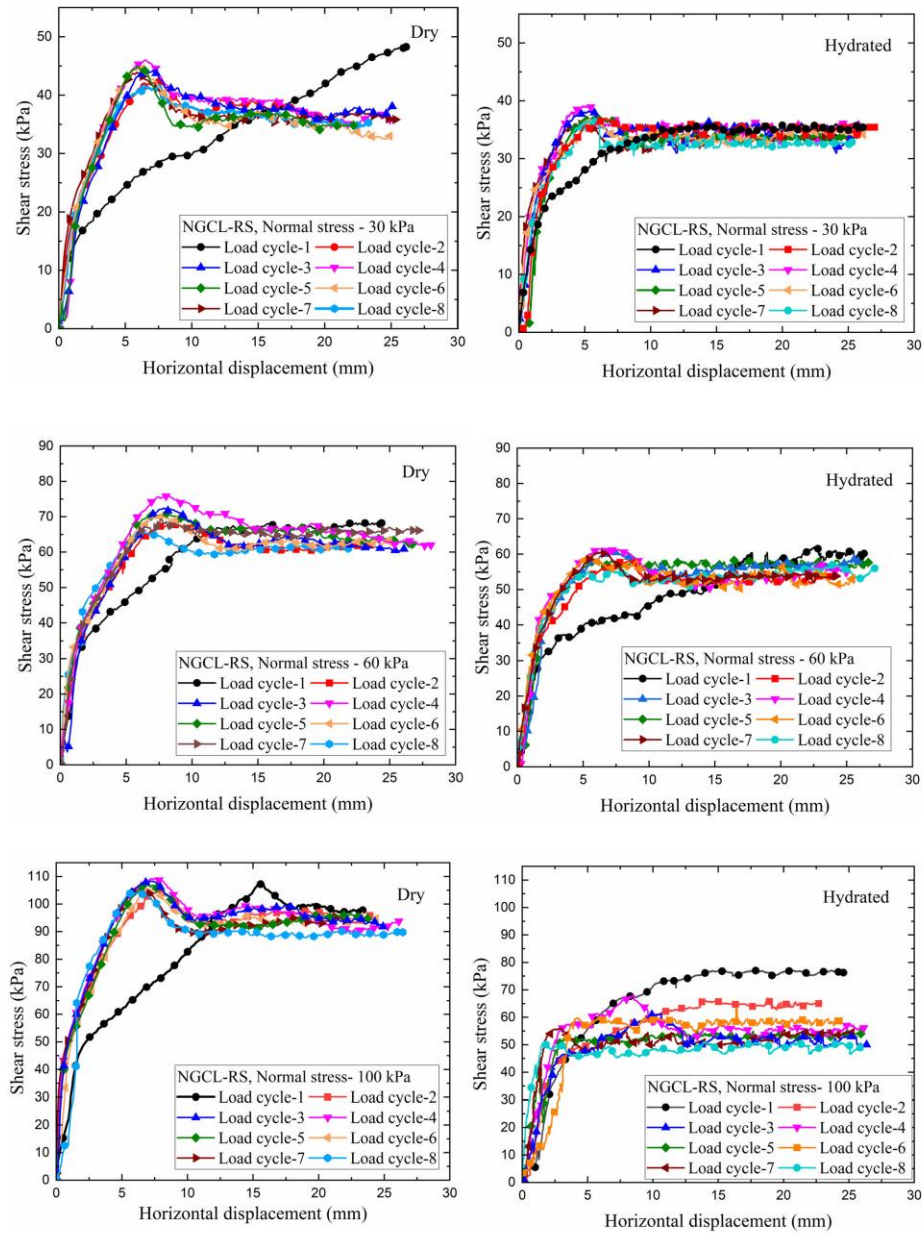


Figure 8

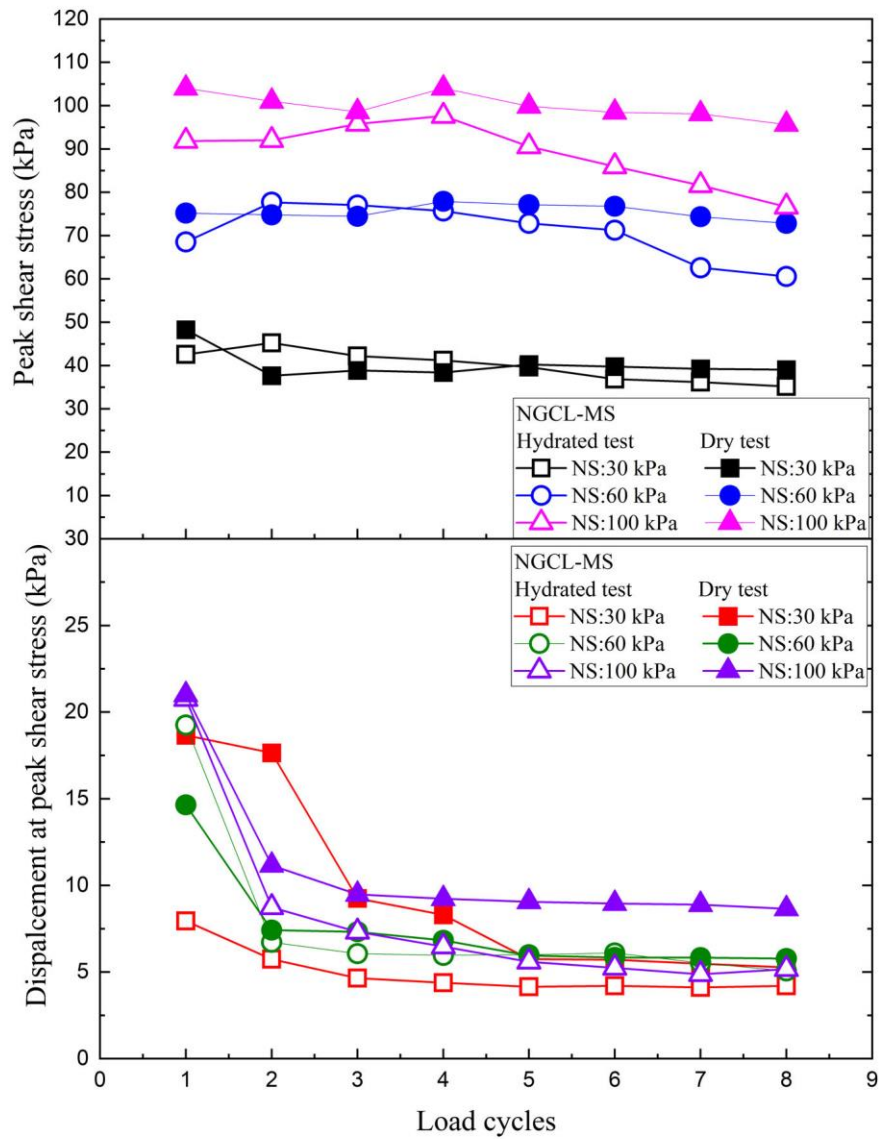


Figure 9

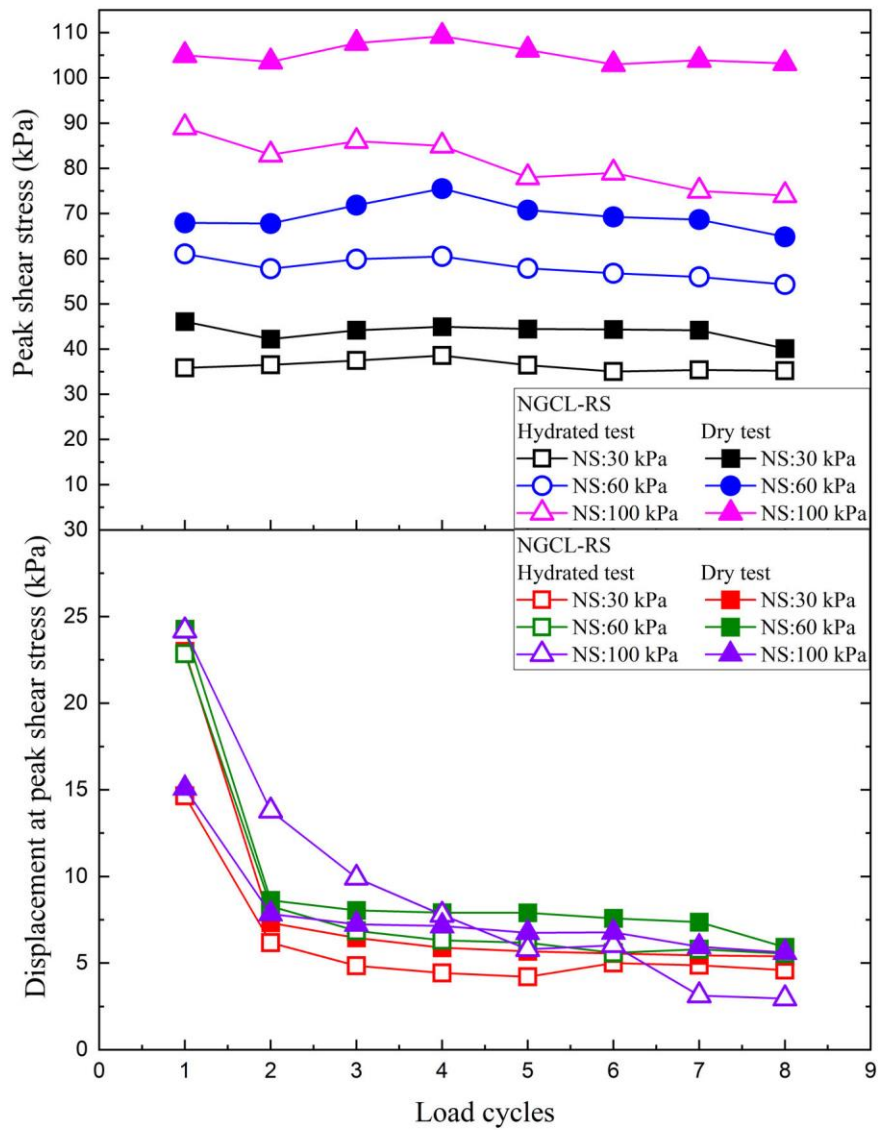


Figure 10

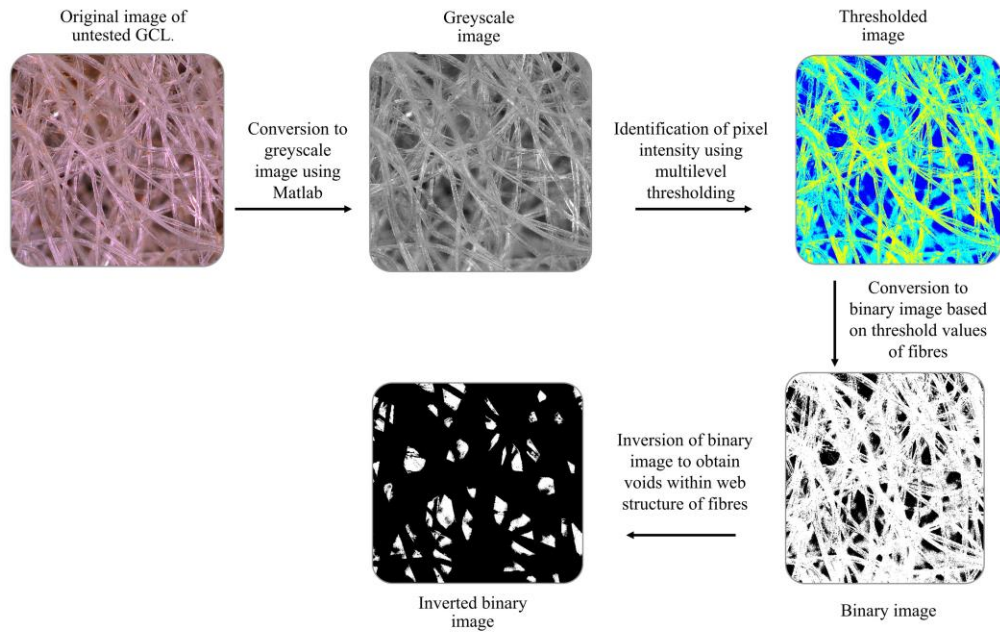


Figure 11

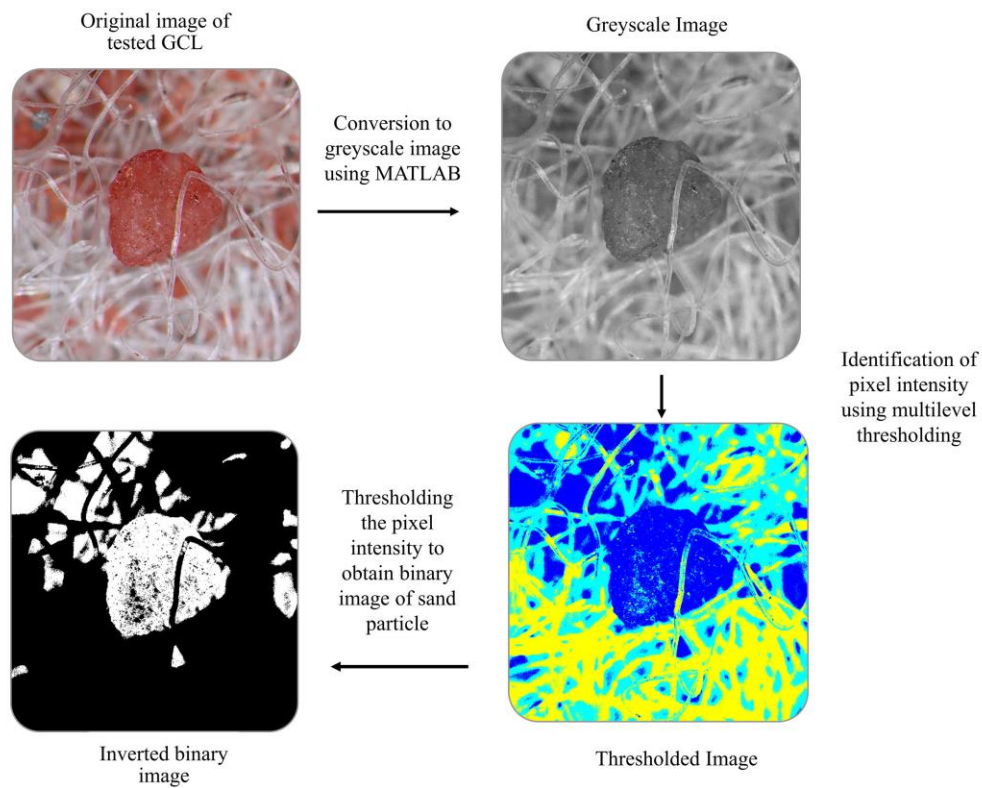


Figure 12

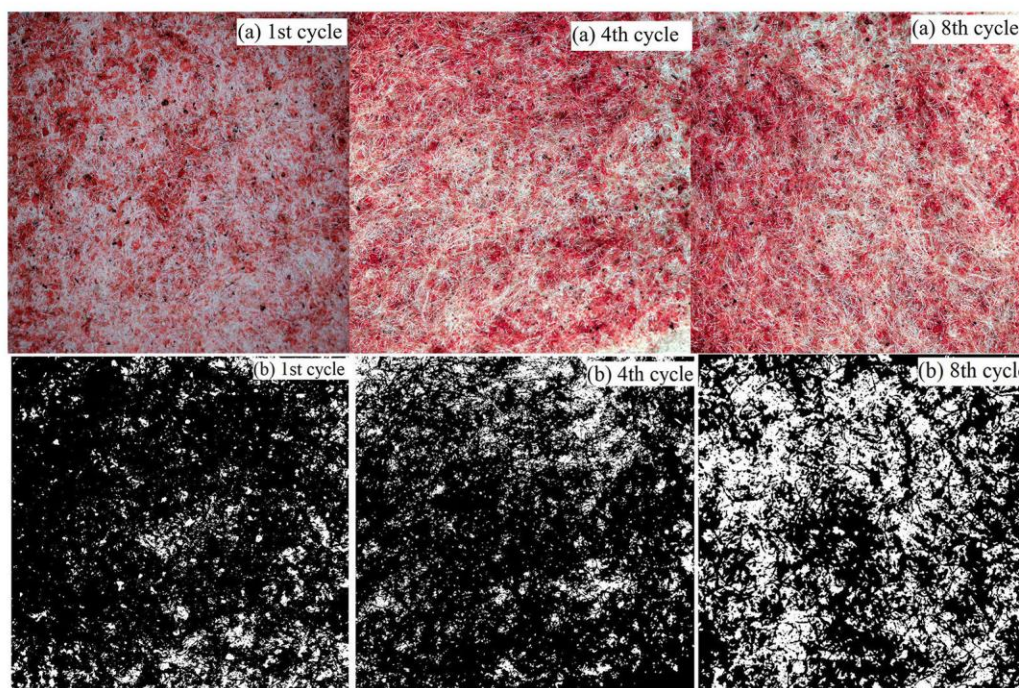


Figure 13

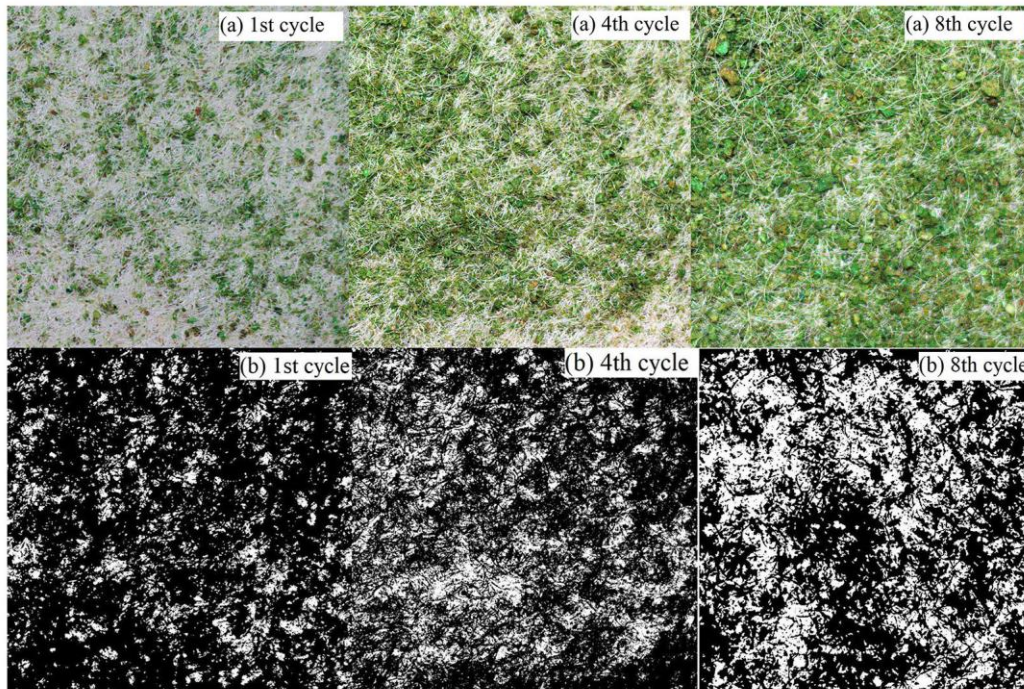


Figure 14

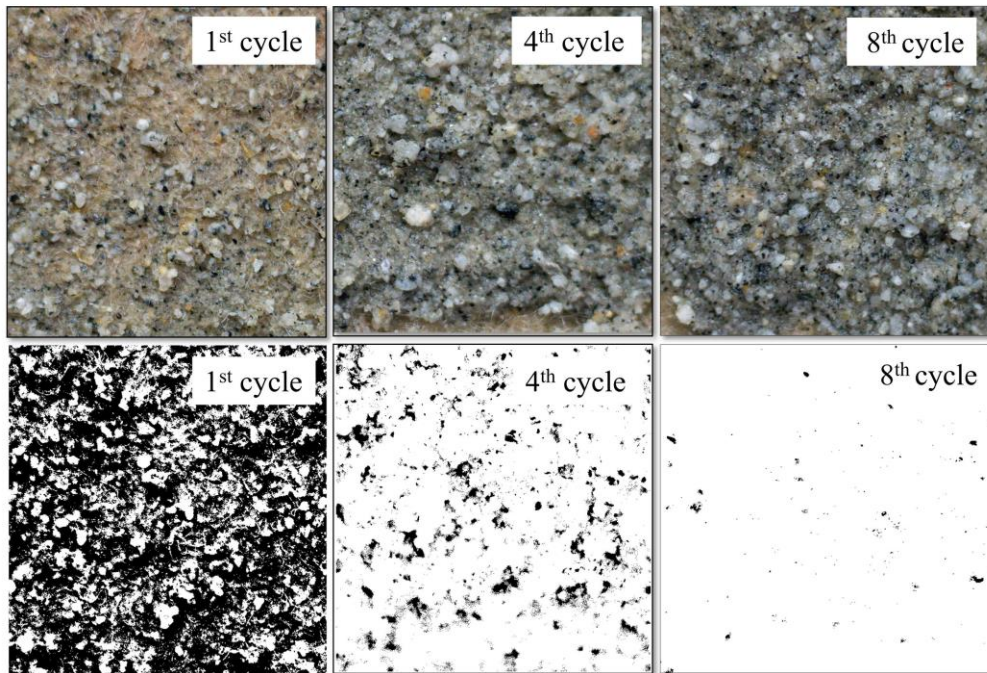


Figure 15

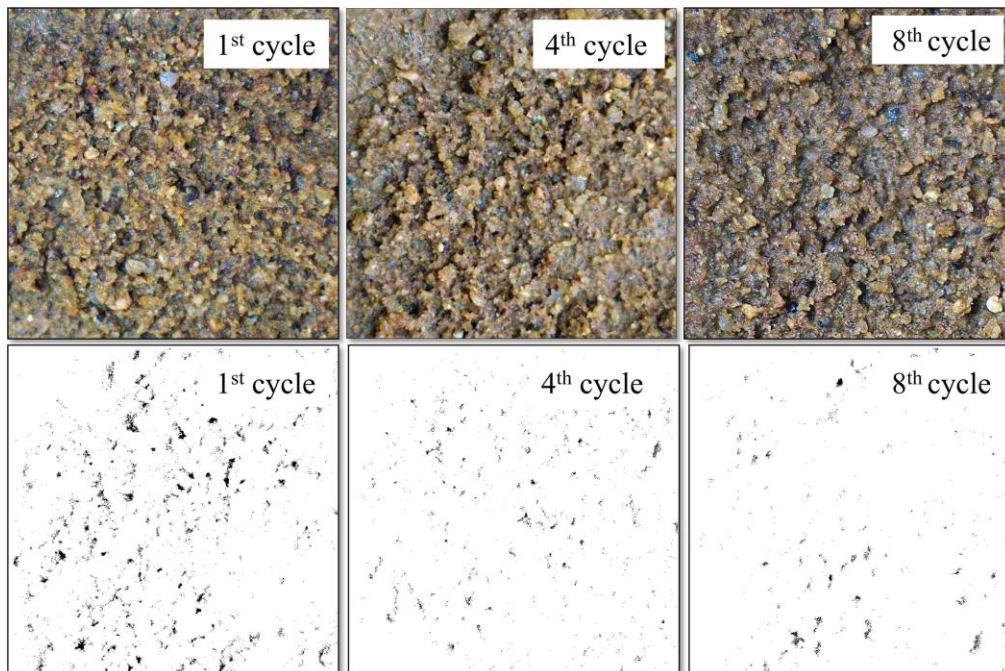


Figure 16

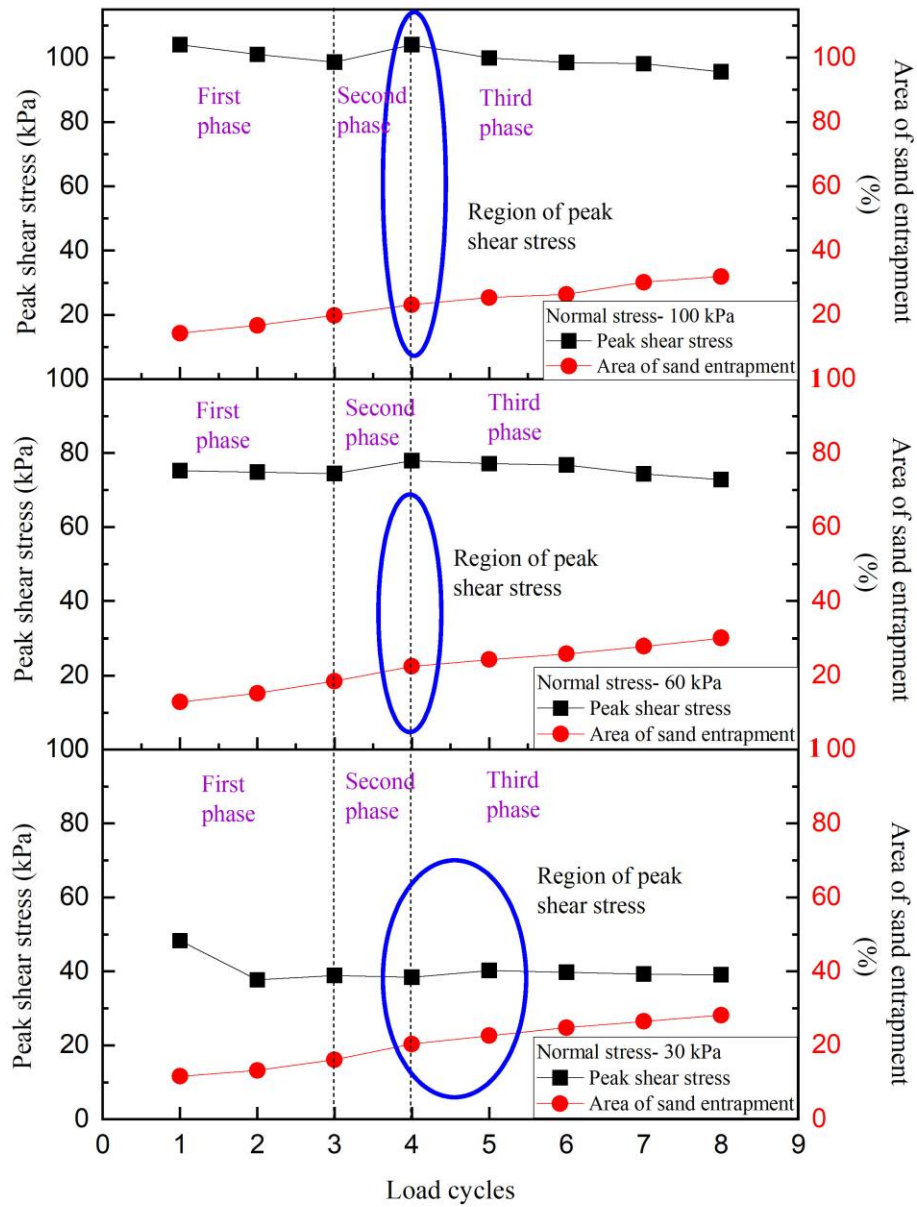


Figure 17

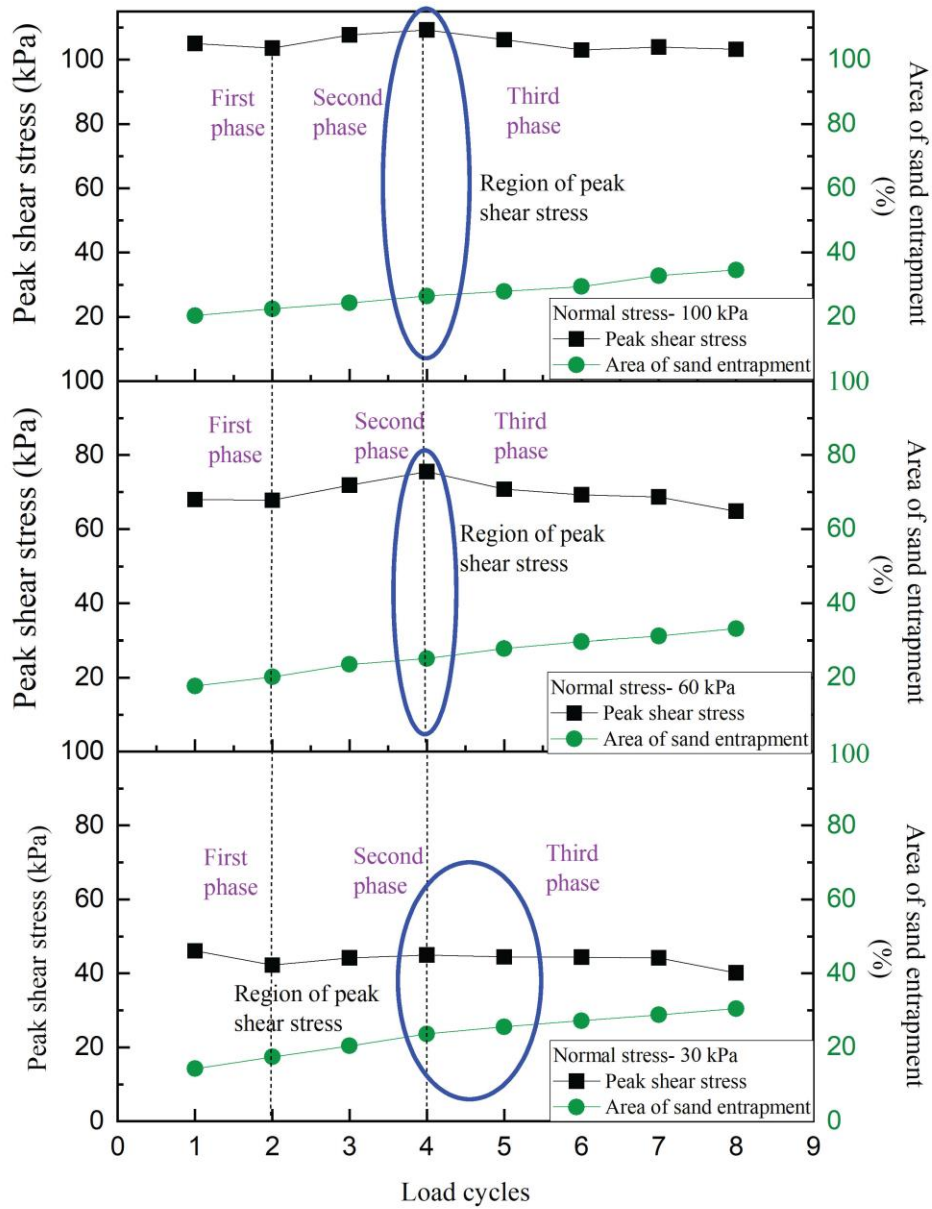


Figure 18

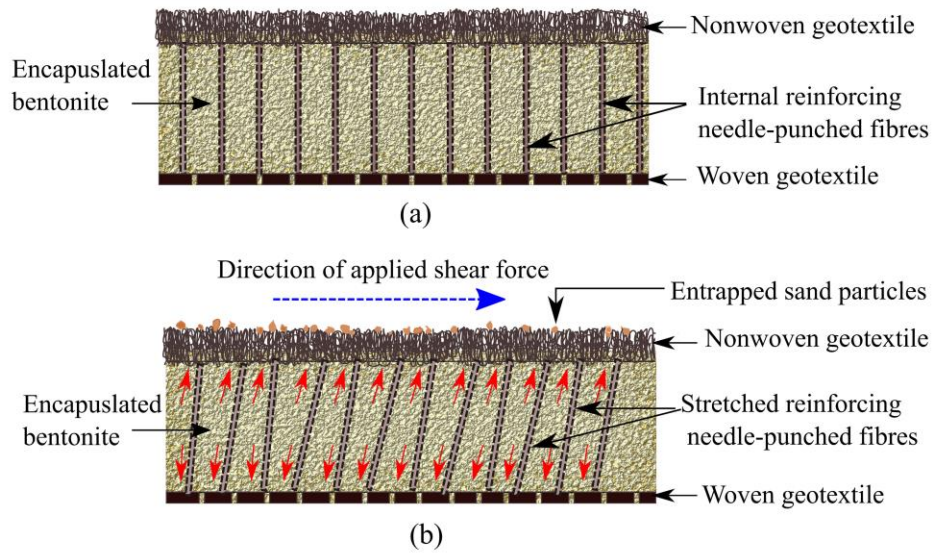


Figure 19



Figure 20

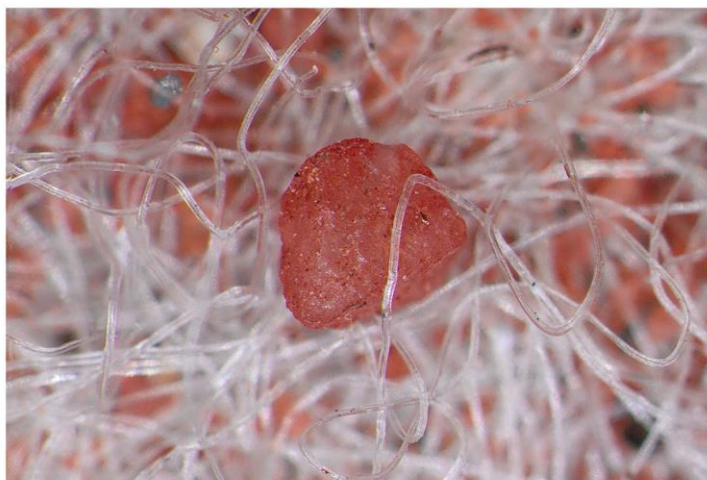


Figure 21

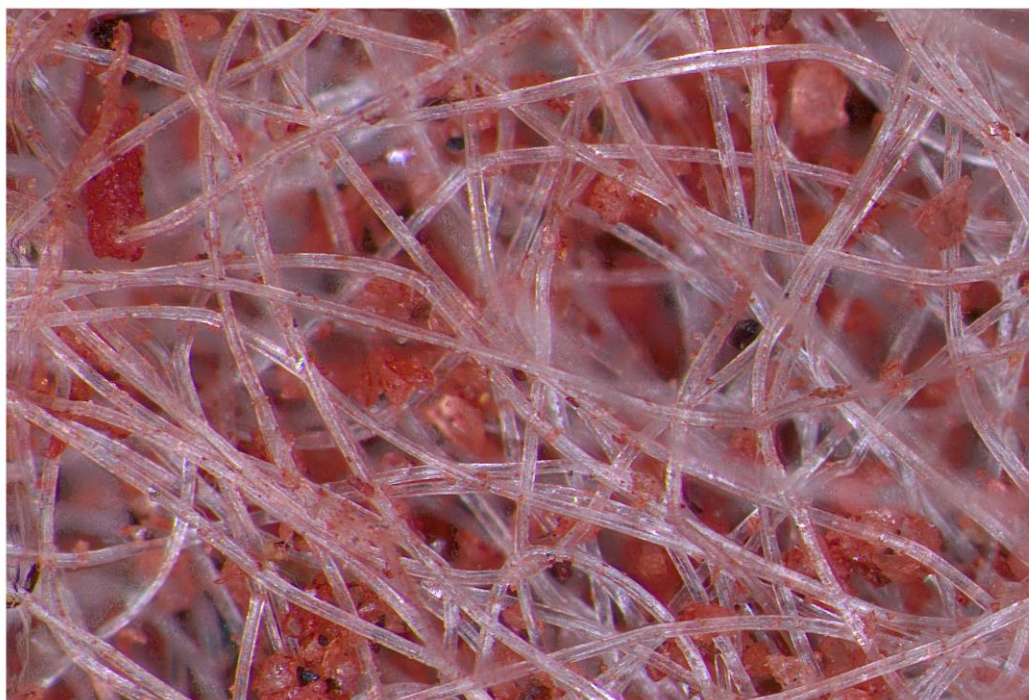


Figure 22

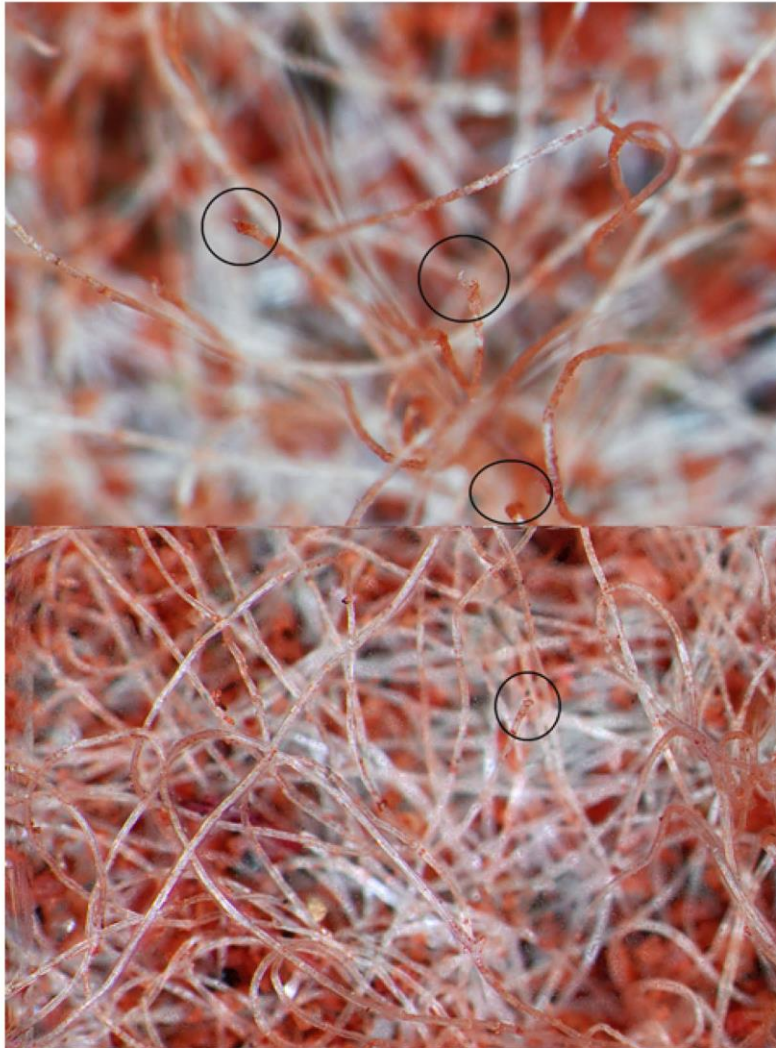


Figure 23

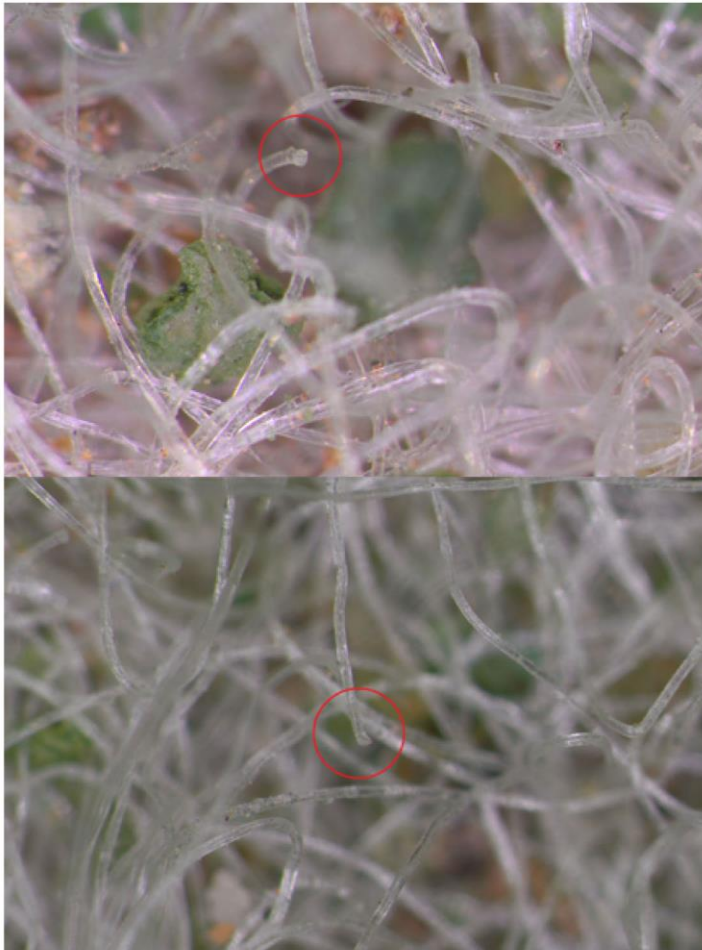


Figure 24

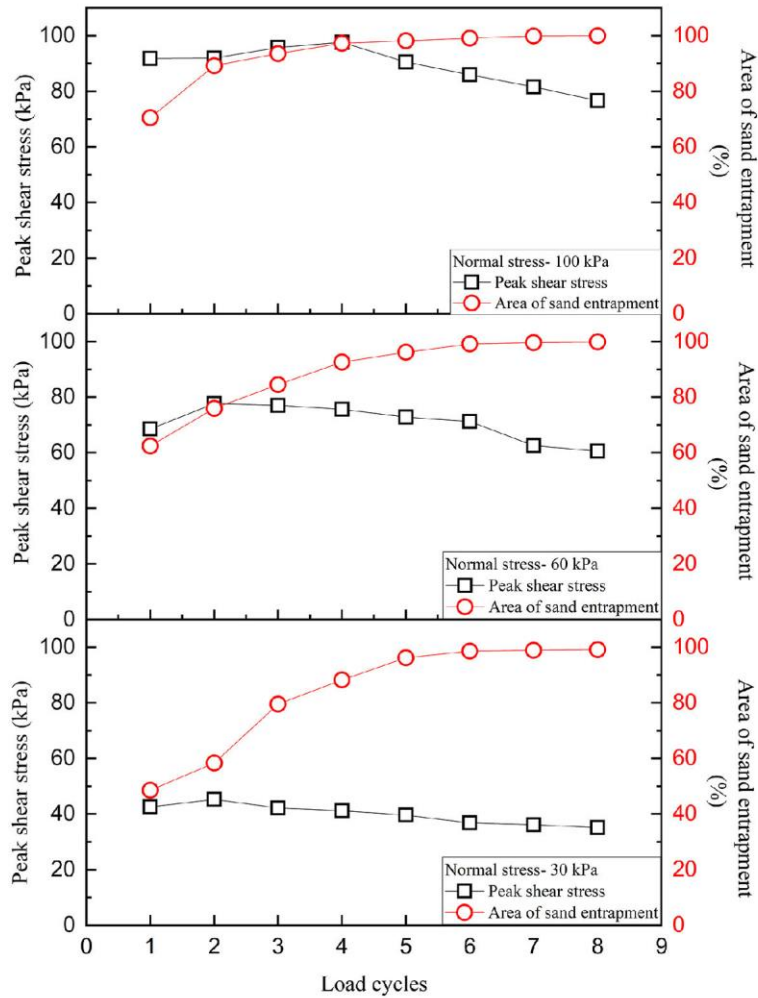


Figure 25

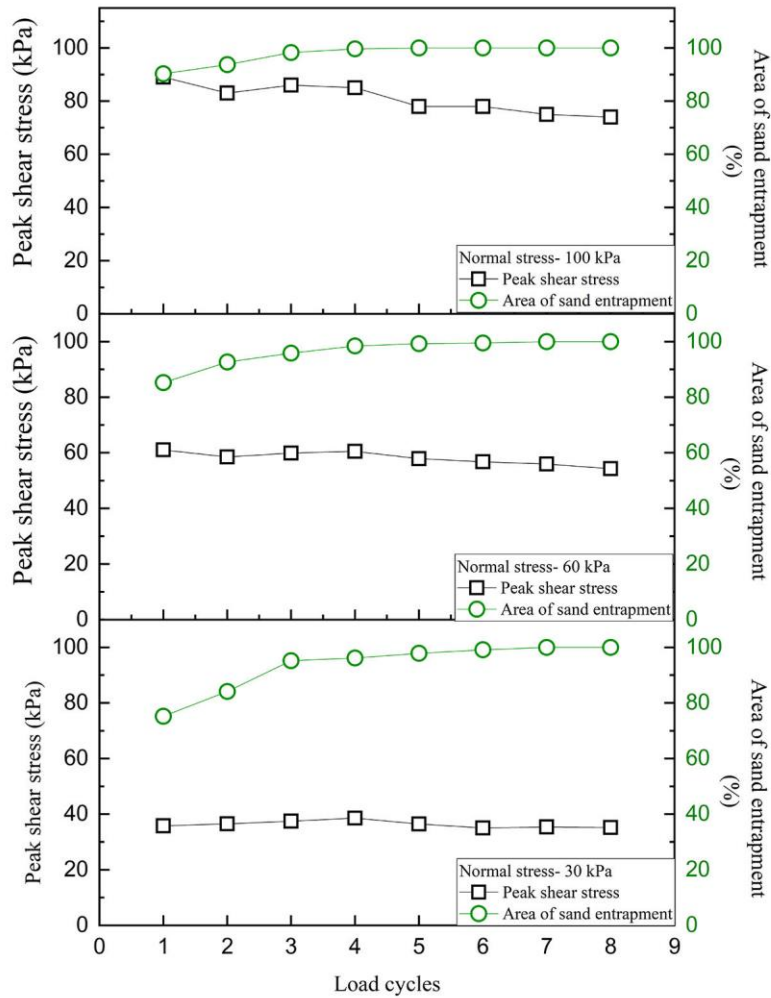


Figure 26

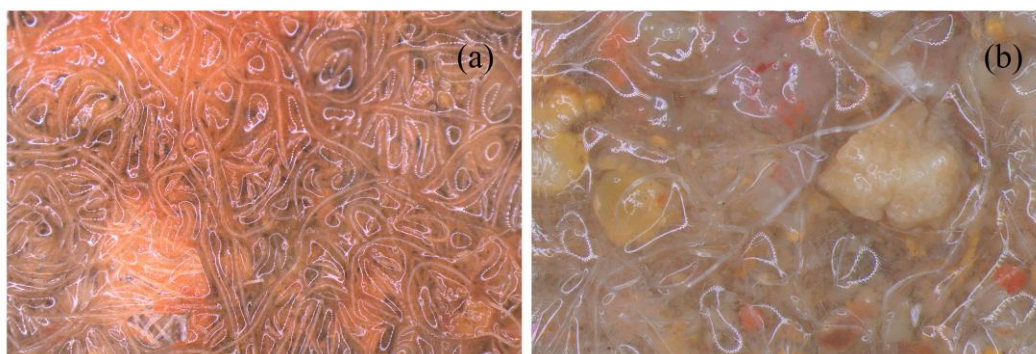


Figure 27